

# The Radio-Gamma Correlation In Starburst Galaxies

B. Eichmann<sup>1</sup> and J. Becker Tjus<sup>1</sup>

*Institut für Theoretische Physik, Lehrstuhl IV: Plasma-Astroteilchenphysik, Ruhr-Universität  
Bochum, 44780 Bochum, Germany*

## Abstract

We present a systematic study of the non-thermal electron-proton plasma and its emission processes in starburst galaxies in order to explain the correlation between the luminosity in the radio band and the recently observed gamma luminosity. In doing so, a steady state description of the non-thermal electrons and protons within the spatially homogeneous starburst is considered where continuous momentum losses are included as well as catastrophic losses due to diffusion and advection. The primary source of the relativistic electron-proton plasma, e.g. supernova remnants, provides a quasi-neutral plasma with a power law spectrum in momentum where we account for rigidity dependent differences between the electron and proton spectrum. We examine the resulting leptonic and hadronic radiation processes by synchrotron radiation, inverse Compton scattering, Bremsstrahlung and hadronic pion production.

Finally, the observations of NGC 253, M 82, NGC 4945 and NGC 1068 in the radio and gamma-ray band are used to constrain a best-fit model, that is subsequently used to determine the corresponding supernova rate, the calorimetric behavior as well as the expected neutrino flux. It is shown that the primary electron source spectrum at high energies needs to be steepened by inverse Compton (or synchrotron) losses. Furthermore, secondary electrons are important to model the radio flux, especially in the case of M 82. Another important result is that supernovae can not be the dominant source of relativistic particles in NGC 4945 and NGC 1068 and the relativistic particle outflow in all considered starburst galaxies consists of protons that are driven by the diffusion.

## 1. Introduction

The far infrared (FIR) emission is a common indicator of the star formation rate (SFR) in galaxies. Here, an almost constant ratio between the FIR and the radio emission has been established (Helou et al. (1985)) in galaxies with a high SFR, so-called starburst galaxies. In the following, several photometric SFR estimators have been suggested like the radio continuum luminosity at

---

<sup>1</sup>Institut für Theoretische Physik, Lehrstuhl IV: Weltraum- und Astrophysik, Ruhr-Universität Bochum, 44780 Bochum, Germany

1.4 GHz (Yun et al. (2001)). To date, four starburst galaxies (M 82, NGC 253, NGC 1068 and NGC 4945) have also been detected in the  $\gamma$ -ray by the Fermi LAT (Abdo et al. (2010), Lenain et al. (2010)) without showing indications of gamma-ray variability (Ackermann et al. (2012)). These galaxies show evidence that there is also a quasi-linear scaling relation between the gamma-ray luminosity and the radio continuum luminosity (Ackermann et al. (2012)). However, only M 82 and NGC 253 (with some problems modeling the radio data of the latter) have been described by a self-consistent model (Yoast-Hull et al. (2013), Yoast-Hull et al. (2014)) so far.

The FIR emission is supposed to mainly represent star light absorbed and re-radiated by dust. The radio emission is well explained by synchrotron radiation of relativistic electrons, so that the FIR–radio correlation mainly depends on the average photon and magnetic field energy density  $U_{rad}$  and  $U_B$ , respectively, according to  $1 + U_{rad}/U_B$  (Völk (1989)). In contrast to the FIR and radio emission, is the origin of the  $\gamma$ -ray emission still under debate. On the one hand, leptonic scenarios like inverse Compton (IC) or non-thermal Bremsstrahlung are anticipated as vital processes. But on the other hand, a hadronic scenario like hadronic pion production is mostly favored as the dominant  $\gamma$ -ray emission process. The basic requirement in order to obtain gamma-ray emission is an efficient particle acceleration mechanism within the starburst. A common explanation for the high energetic cosmic rays (CRs) within the galaxy is the acceleration in supernova remnant shock fronts. However, an other possible source of the accelerated particles in starburst galaxies with an active galactic nucleus (indicated by jet-like structures, as observed in NGC 1068 and NGC 4945) could correspond to the central engine. Without knowing the details of the acceleration process, we still take the rigidity dependent differences between electrons and protons into account.

Galactic winds with wind speeds of at least a few 100 km s<sup>−1</sup> (e. g. Westmoquette et al. (2011), Stevens et al. (2003), Shopbell and Bland-Hawthorn (1998)) are often supposed to be another important constituent of starburst galaxies. Due to the advection of particles out of the starburst, these winds can have an important influence on the emitted radiation as exposed in previous calculations (e.g. Yoast-Hull et al. (2013), Yoast-Hull et al. (2014)). However, we will show that ultrarelativistic protons are more affected by the diffusion process, so that diffusion is an important ingredient in order to determine the gamma-ray flux of starburst galaxies.

In this paper we present a theoretical model that describes the emission of the spherical symmetric and spatially homogeneous part of a starburst galaxy. This is an appropriate assumption, since we have no a priori knowledge about the spatial and temporal distribution of the particle accelerators, the magnetic fields or the thermal particles in starburst galaxies. Furthermore, possible small-scale inhomogeneities vanish on scales much larger than the gyroradius  $r_L$  of the particles.

In contrast to previous calculations (e.g. Yoast-Hull et al. (2013), Yoast-Hull et al. (2014)) we take the impact of continuous momentum losses as well as advection and diffusion on the relativistic particle spectrum into account. In particular, the flattening of the continuous energy loss rate of hadronic pion production at proton energies  $> 200$  GeV (Krakau and Schlickeiser (2015)) is included. Additionally, we keep the total source of the relativistic particles as general as possible, but account for differences between the source spectrum of accelerated electrons and protons.

First of all, Section 2 presents the solution of the transport equation of relativistic electrons and

protons within the starburst. In Section 3 the relativistic electrons are used to determine the emergent synchrotron radiation, whereas in Section 4 the resulting  $\gamma$ -radiation from hadronic pion production, Inverse Compton scattering and Bremsstrahlung are determined. Furthermore, the secondary neutrinos and electrons that result from the  $\pi^\pm$ -decay are calculated. The data of the gamma-ray and radio flux of four starburst galaxies that have recently been observed in the  $\gamma$ -ray band is used in Section 5. Here, we constrain the possible magnetic field strength  $B$ , target density  $N_t$ , galactic wind speed  $v_{adv}$ , diffusion length  $l_e$  as well as the initial source spectrum. Finally, the best-fit model is used to determine the corresponding rate of supernova (SN) explosions, the influence of secondary electrons, the calorimetric behavior and the neutrino flux of these starburst galaxies.

## 2. Steady state particle transport equation

Starburst galaxies show no hints of temporal variability (Ackermann et al. (2012)), so that the relativistic electrons and protons within the starburst can be considered in their steady state. Furthermore, we suppose them to be spatially homogeneous and isotropic due to the mathematical convenience and the lack of information. Thus, spatial diffusion effects can be simplified by the leaky-box approach, where only the retarding effect on the escape time of the electrons is considered. Additionally, the effects of galactic winds are considered due to the advection of particles and magnetic fields. Furthermore, the relativistic particles suffer continuous momentum losses (with a loss rate  $|\dot{\gamma}|_{e,p}$ ). Consequently, the differential particle density of relativistic electrons and protons  $n_{e,p}$  can be described by

$$0 = \frac{\partial}{\partial \gamma} (|\dot{\gamma}|_{e,p} n_{e,p}) - \frac{n_{e,p}}{\tau_{diff}^{e,p}(\gamma)} - \frac{n_{e,p}}{\tau_{adv}} + q_{e,p}(\gamma), \quad (1)$$

where  $q_{e,p}(\gamma)$  takes an energy dependent source rate of electrons and protons, respectively, into account. The particle acceleration is supposed to be decoupled from the considered radiation region of the starburst galaxy. Since the energy distribution of the source rate is a major ingredient in matters of the resulting radiation spectrum, a straight power-law spectrum can be oversimplified. Diffusive shock acceleration is the favored acceleration mechanism of supernova remnants which are usually assumed to be the main source of the relativistic particles. The resulting power-law spectrum according to diffusive shock acceleration has a spectral index of around  $-2$  (dependent on the compression ratio of the shocked gas). However, the maximum energy of the resulting energy spectrum depends on the rigidity of the particle and furthermore, ultrarelativistic electrons are more susceptible to continuous momentum losses than protons. Latter is supported by recent particle-in-cell simulations (Park et al. (2015)) showing that the energy gain of electrons is faster than the energy gain of protons and hence, the electrons faster reach an energy where continuous momentum losses become significant. In addition, it is later shown that the dominant cooling mechanism of the ultrarelativistic protons is hadronic pion production, which hardly changes the spectral shape of the energy distribution.

The total number of accelerated protons and electrons is supposed to be equal in order to provide a quasi-neutral electron-proton plasma.

Besides the continuous energy losses in the transport eq. (1) there are catastrophic losses according to diffusion and advection of particles considered. In doing so, the diffusion timescale is approximated by (e.g. Prölss and Bird (2004))

$$\tau_{diff}(\gamma) \simeq \frac{R^2}{3D(\gamma)} \simeq \frac{R^2}{cl_{e,p}} \gamma^{-\beta}, \quad (2)$$

where a diffusion coefficient  $D(\gamma) = cl_{e,p} \gamma^\beta / 3 \propto r_L^\beta$  has been adopted with a corresponding mean free path  $l_{e,p} \gamma^\beta$  of electrons and protons, respectively. According to the mass dependent Larmor radius  $r_L$  we obtain  $l_p = l_e (m_p/m_e)^\beta$  (Schlickeiser (2001)) and  $\beta = 1/3$  for Kolmogorov diffusion, whereas  $\beta = 1$  in the case of Bohm diffusion. The mean free path  $l_e$  generally depends on the turbulence spectrum of the plasma waves that scatter the particles as well as the square of the ratio between background magnetic field strength and magnetic turbulence. As these information are observationally inaccessible radio observations are used to evaluate the diffusion coefficient (Heesen et al. (2009), Berezhinskii et al. (1990)) suggesting

$$D(E) \simeq 10^{(28-29)} \left( \frac{E}{1 \text{ GeV}} \right)^{1/3} \text{ cm}^2 \text{ s}^{-1}, \quad (3)$$

so that  $l_e = 8.2 \cdot 10^{(16-17)} \text{ cm}$  and  $\beta = 1/3$ .

The timescale of advection  $\tau_{adv}$  is determined by the galactic wind speed  $v_{adv}$  which is supposed to be a constant in the order of a few hundred km/s, so that  $\tau_{adv} \simeq R/v_{adv}$ .

Consequently, in the case of a galactic wind speed of

$$v_{adv} \leq \frac{3D(E)}{R} = 4.9 \cdot 10^{(7-8)} R_{200}^{-1} \left( \frac{E}{1 \text{ GeV}} \right)^{1/3} \text{ cm/s} \quad (4)$$

the relativistic particles are predominantly affected by the diffusion process and not by the galactic wind (see fig. 1). Here as well as in the following a spherical symmetric starburst with a radius  $R = 200 R_{200} \text{ pc}$  is supposed. In general, diffusion and advection losses need to be taken into account in order to determine accurately the whole energy spectrum of the relativistic particles. However, the relativistic protons are predominantly affected by the diffusion losses.

Starburst galaxies are generally extremely bright at infrared wavelengths with  $L_{IR} = 3.85 \cdot 10^{43} L_{43} \text{ erg s}^{-1}$ , where  $L_{43} \sim 1 - 10$  (Telesco and Harper (1980)), so that the appropriate energy density yields  $U_{IR} = 2.7 \cdot 10^{-10} L_{43} R_{200}^{-2} \text{ erg cm}^{-3}$ . Furthermore, the high SFR in starburst galaxies also implicates a high density of target particles  $N_t \gg 1 \text{ cm}^{-3}$  as well as a magnetic field strength  $B$  in the order of a few  $10 \mu\text{G}$  up to a few  $\text{mG}$ .

It is shown in the Appendix A, that the general solution of the transport equation (1) is given by

$$n_{e,p}(\gamma) = \exp \left( \int \frac{d\gamma}{|\dot{\gamma}|_{e,p} \tau_{adv}} \right) e^{-\zeta_0^{e,p}(\gamma)} \int_{\gamma}^{\gamma_{max}} d\gamma' \frac{q_{e,p}(\gamma')}{|\dot{\gamma}'|_{e,p}} e^{\zeta_0^{e,p}(\gamma')} \exp \left( - \int \frac{d\gamma'}{|\dot{\gamma}'|_{e,p} \tau_{adv}} \right), \quad (5)$$

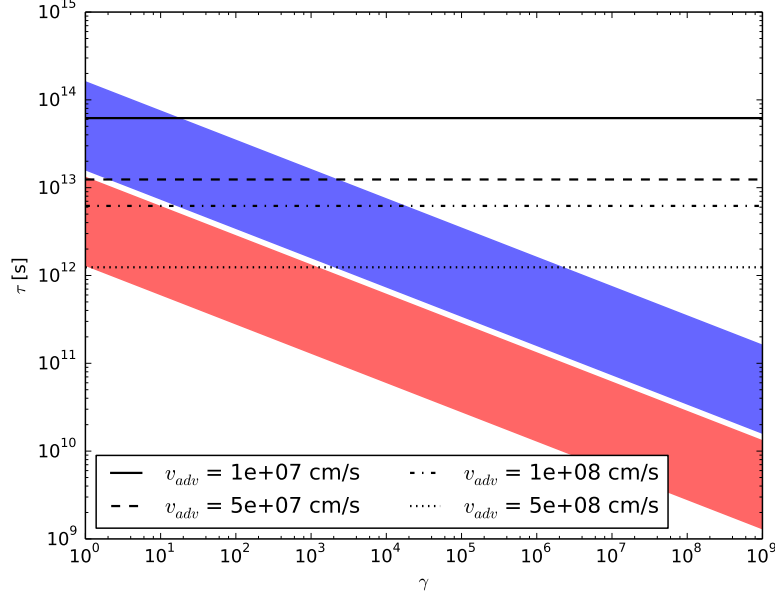


Fig. 1.—: Range of the diffusive loss timescale  $\tau_{diff}$  of electrons (blue) and protons (red) as well as the timescales of advection  $\tau_{adv}$  (black) for four different galactic wind speeds.

where

$$\zeta_0^{e,p}(\gamma) = \int d\gamma \frac{1}{|\dot{\gamma}|_{e,p}} \frac{\partial |\dot{\gamma}|_{e,p}}{\partial \gamma} - \frac{1}{\tau_{diff}^{e,p}(\gamma) |\dot{\gamma}|_{e,p}}. \quad (6)$$

In the following, the general solution (5) is specified by the individual interactions of relativistic electrons and protons with their environment.

## 2.1. Solution of the electron transport equation

In the case of relativistic electrons, the continuous momentum losses are determined by synchrotron, inverse Compton (IC), Bremsstrahlung and ionization losses. We consider the IC losses only in the Thomson limit, where the energy  $\epsilon$  of the scattered infrared photon satisfies  $\epsilon \gamma \ll m_e c^2$ . In general, ultra-relativistic electrons with  $\gamma > m_e c^2 / \epsilon$  are in the Klein-Nishina (KN) regime, where the electrons lose a sizeable fraction of their energy by a Compton collision. Although, only a small amount of the injected power-law distributed electrons are within the KN regime, we consider a maximal initial Lorentz factor of  $\gamma_{max}^e = 10^8$ , caused by the IC losses in the KN regime (see fig. 2). Hence, the maximal Lorentz factor of electrons is not given by the particle accelerator but the onset of IC losses in the KN regime.

Thus, the total loss rate of relativistic electrons is determined by

$$|\dot{\gamma}|_e \simeq (\Lambda_{syn} + \Lambda_{IC}) \gamma^2 + \Lambda_{Br} \gamma + \Lambda_{io,e}, \quad (7)$$

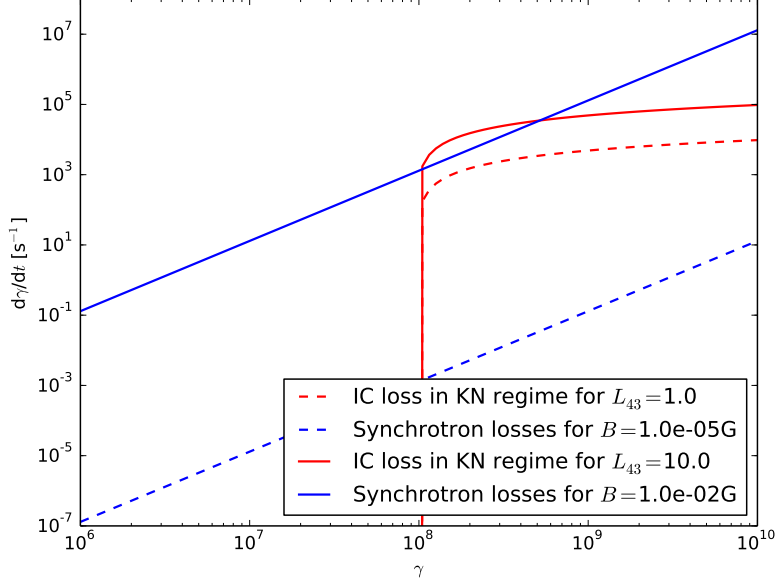


Fig. 2.—: Loss rate of relativistic electrons according to synchrotron radiation as well as IC collisions in the KN regime (Schlickeiser (2001)).

where

$$\Lambda_{syn} \simeq 1.3 \cdot 10^{-9} \left( \frac{B}{\text{Gauss}} \right)^2 \text{ s}^{-1}, \quad (8)$$

$$\Lambda_{IC} \simeq 8.6 \cdot 10^{-18} L_{43} R_{200}^{-2} \text{ s}^{-1}, \quad (9)$$

$$\Lambda_{Br} \simeq 10^{-15} \left( \frac{N_t}{\text{cm}^{-3}} \right) \text{ s}^{-1}, \quad (10)$$

and

$$\Lambda_{io,e} \simeq 7.2 \cdot 10^{-13} \left( \frac{N_t}{\text{cm}^{-3}} \right) \text{ s}^{-1}. \quad (11)$$

Here,  $N_t$  denotes the particle density of the target plasma and  $B$  refers to the magnetic field strength.

In the following, the diffusion timescale (2) and the total relativistic energy loss term (7) is used, so that the  $\zeta_0^e$ -term (6) yields

$$\zeta_0^e(\gamma) = \ln \left( \frac{(\Lambda_{syn} + \Lambda_{IC}) \gamma^2 + \Lambda_{Br} \gamma + \Lambda_{io}}{\Lambda_{syn} + \Lambda_{IC}} \right) - I_{diff}^e(\gamma), \quad (12)$$

with

$$\begin{aligned}
I_{diff}^e(\gamma) &= \frac{cl_e}{R^2(\Lambda_{syn} + \Lambda_{IC})} \int d\gamma \frac{\gamma^\beta}{\gamma^2 + \Lambda_1 \gamma + \Lambda_2} \\
&= \frac{2^{-\beta} cl_e}{R^2(\Lambda_{syn} + \Lambda_{IC})} \left( \beta \sqrt{\Lambda_1^2 - 4\Lambda_2} \right)^{-1} \\
&\quad \times \left[ \left( \frac{\gamma}{\Lambda_1 + 2\gamma - \sqrt{\Lambda_1^2 - 4\Lambda_2}} \right)^{-\beta} {}_2F_1 \left( -\beta, -\beta; 1 - \beta; \frac{\Lambda_1 - \sqrt{\Lambda_1^2 - 4\Lambda_2}}{\Lambda_1 + 2\gamma - \sqrt{\Lambda_1^2 - 4\Lambda_2}} \right) \right. \\
&\quad \left. - \left( \frac{\gamma}{\Lambda_1 + 2\gamma + \sqrt{\Lambda_1^2 - 4\Lambda_2}} \right)^{-\beta} {}_2F_1 \left( -\beta, -\beta; 1 - \beta; \frac{\Lambda_1 + \sqrt{\Lambda_1^2 - 4\Lambda_2}}{\Lambda_1 + 2\gamma + \sqrt{\Lambda_1^2 - 4\Lambda_2}} \right) \right], \tag{13}
\end{aligned}$$

where

$$\Lambda_1 = \frac{\Lambda_{Br}}{(\Lambda_{syn} + \Lambda_{IC})} \quad \text{and} \quad \Lambda_2 = \frac{\Lambda_{io}}{(\Lambda_{syn} + \Lambda_{IC})}, \tag{14}$$

and  ${}_2F_1(a, b; c; x)$  denotes the hypergeometric function.

In order to determine the relativistic electron density (5), the source term  $q_e(\gamma)$  needs to be specified: First, there are primary electrons related to a source rate  $q_{e1}(\gamma)$  due to the particle accelerators that are supposed to be homogeneously distributed within the starburst. Thus, in steady state we obtain a power-law distributed spectrum in momentum space with a spectral index  $\alpha$  between  $p_{min} = m_e c \sqrt{\gamma_{min}^2 - 1}$  and  $p_{max} = m_e c \sqrt{\gamma_{max}^2 - 1}$ . Based on the dense IR photon fields within the starburst galaxy, the primary electron source spectrum is already effected by IC losses when  $|\dot{\gamma}|_{IC} \geq |\dot{\gamma}|_{acc}$ . We suppose a strong shock, so that the ratio of the upstream to downstream plasma velocity yields  $u_u/u_d = 4$ . Furthermore, the diffusion coefficient on both sides of the shock is assumed to equal the diffusion coefficient  $D(\gamma) = cl_{e,p}\gamma^\beta/3$  within the starburst galaxy. Hence, the timescale  $\tau_{cycle}$  for one back-and forth encounter yields (Gaisser (1990))

$$\tau_{cycle} = \frac{20}{3} \frac{l_{e,p} \gamma^\beta}{u_u}. \tag{15}$$

With an average fractional energy gain per encounter of  $\xi = u_u/c$  according to the first order Fermi acceleration, the continuous energy gain is determined by

$$|\dot{\gamma}|_{acc} = \frac{\xi \gamma}{\tau_{cycle}} = \frac{3}{20} \frac{u_u^2}{c} l_{e,p}^{-1} \gamma^{1-\beta}. \tag{16}$$

In the lab frame, the upstream velocity  $u_u$  equals the shock velocity  $u_s$ , which is given by  $u_s = 5 \cdot 10^8 u_5 \text{ cm/s}$ . Thus, the primary electron source spectrum is dominated by IC losses for

$$\gamma > \gamma_B \equiv \left[ 1.5 \cdot 10^{23} \left( \frac{l_e}{1 \text{ cm}} \right)^{-1} u_5^2 L_{43}^{-1} R_{200}^2 \right]^{\frac{1}{1+\beta}}. \tag{17}$$

Here, the energy spectrum with a spectral index of  $\alpha$  steepens to  $\alpha - 1$  due to the IC losses. Note, that the consideration of the continuous synchrotron losses instead of the IC losses lead to the same

results for  $B = 81 L_{43}^{1/2} R_{200}^{-1} \mu\text{G}$ . But it needs to be taken into account that an increasing magnetic field strength is also supposed to increase the acceleration rate (16) since  $l_e \propto (r_L/\gamma)^\beta \propto B^{-\beta}$ . As the details of the acceleration mechanism are still unknown and several assumptions have been made in order to determine eq. (17), we will subsequently treat  $A = \gamma_B^{-1}$  as a free parameter. The resulting  $\gamma$ -ray flux contribution of the accelerator to the total gamma radiation can be neglected as the lifetime  $T_A \sim 1000$  yrs of the accelerator (Gaisser (1990)) is much smaller than the duration of stay within the starburst galaxy (see fig. 1).

Secondly, there is a contribution by secondary electrons with a rate  $q_{e2}(\gamma)$  due to the hadronic pion production of the relativistic protons as shown in Section 4.4.

In total, the source rate of relativistic electrons yields

$$q_e(\gamma) = q_{e1}(\gamma) + q_{e2}(\gamma) = q_0^e \gamma [\gamma^2 - 1]^{-\frac{\alpha+1}{2}} (1 + A\gamma)^{-1} H[\gamma - \gamma_{min}] H[\gamma_{max}^e - \gamma] + q_{e2}(\gamma), \quad (18)$$

where  $A \simeq \gamma_B^{-1}$  denotes a dimensionless parameter that account for the steepening of the spectrum at  $\gamma_B$ . Note, that the break Lorentz factor  $\gamma_B$  strongly depends on the acceleration mechanism. Hence, the relativistic electron density depends on the relativistic proton density due to the source rate  $q_{e2}(\gamma)$  of secondary electrons. Using the sum of the primary and secondary source rate, the loss term (7), as well as the eq. (12) we obtain the relativistic electron density

$$n_e(\gamma) = ((\Lambda_{syn} + \Lambda_{IC}) \gamma^2 + \Lambda_{Br} \gamma + \Lambda_{io})^{-1} \exp(I_{diff}^e(\gamma) + F_{adv}^e(\gamma)) \times \int_{\gamma_l}^{\gamma_{max}^e} d\gamma' \left( q_0^e \gamma' [\gamma'^2 - 1]^{-\frac{\alpha+1}{2}} + q_{e2}(\gamma') \right) \exp(-(I_{diff}^e(\gamma') + F_{adv}^e(\gamma'))) \quad (19)$$

where the function

$$F_{adv}^e(\gamma) = \frac{2}{\tau_{adv} \sqrt{4(\Lambda_{syn} + \Lambda_{IC})\Lambda_{io} - \Lambda_{Br}^2}} \arctan \left( \frac{2(\Lambda_{syn} + \Lambda_{IC})\gamma + \Lambda_{Br}}{\sqrt{4(\Lambda_{syn} + \Lambda_{IC})\Lambda_{io} - \Lambda_{Br}^2}} \right) \quad (20)$$

determines the effect of particle losses due to advection in the same manner as  $I_{diff}^e(\gamma)$  expresses the particle losses caused by diffusion. The lower integration limit is given by

$$\gamma_l = \begin{cases} \gamma, & \text{for } \gamma_{min} < \gamma < \gamma_{max}^e, \\ \gamma_{min}, & \text{for } \gamma \leq \gamma_{min}. \end{cases} \quad (21)$$

In the following, the minimal Lorentz factor is supposed to be  $\gamma_{min} = 1$ , whereas the maximal Lorentz factor is derived from the onset of KN loss yielding  $\gamma_{max}^e = 10^8$ .

## 2.2. Solution of the proton transport equation

In the case of relativistic protons, the hadronic pion production is the dominant loss mechanism as well as the dominant source of  $\gamma$ -rays as later shown. An alternative hadronic gamma-ray



production scenario is the photohadronic pion production. Here, a minimal Lorentz factor of

$$\gamma_{min}^p \simeq \frac{m_\pi c^2}{2E_{IR}} \left( 1 + \frac{m_\pi}{2m_p} \right) = 7.2 \cdot 10^7 \left( \frac{E_{IR}}{\text{eV}} \right)^{-1}. \quad (22)$$

is needed to generate a pion by a head-on collision of a proton with an infrared photon target in the energy range  $E_{IR} \sim [1 \text{ meV}; 1 \text{ eV}]$ .

The appropriate loss rate of a proton with  $\gamma \simeq \gamma_{min}^p$  can be approximated by (Mannheim and Schlickeiser (1994))

$$|\dot{\gamma}|_{p\gamma} \simeq 19 \left( \frac{U_{IR}}{\text{erg cm}^{-3}} \right) \left( \frac{E_{IR}}{\text{eV}} \right)^{-2} \text{s}^{-1} = 8.2 \cdot (10^{-10} - 10^{-9}) \left( \frac{E_{IR}}{\text{eV}} \right)^{-2} \text{s}^{-1}. \quad (23)$$

On the other hand, hadronic pion production can be approximated by (Krakau and Schlickeiser (2015))

$$|\dot{\gamma}|_{pp} \simeq 4.4 \cdot 10^{-16} \left( \frac{N_t}{\text{cm}^{-3}} \right) \gamma^{1.28} (\gamma + 187.6)^{-0.2} \text{s}^{-1}, \quad (24)$$

so that (at  $\gamma \simeq \gamma_{min}^p$ ) photohadronic interactions are negligible if  $|\dot{\gamma}|_{pp} \gg |\dot{\gamma}|_{p\gamma}$ , i.e.

$$N_t \gg 6.1 \cdot (10^{-3} - 10^{-2}) \left( \frac{E_{IR}}{\text{eV}} \right)^{-0.72} \left( \left( \frac{E_{IR}}{\text{eV}} \right)^{-1} + 2.6 \cdot 10^{-6} \right)^{-0.2} \text{cm}^{-3}. \quad (25)$$

In starburst galaxies the target densities usually satisfy the previous condition (25) and hence, the continuous momentum losses of relativistic protons can be considered to be dominated by hadronic pion production as well as ionization losses at lower energies. In total, we obtain

$$|\dot{\gamma}|_p \simeq \Lambda_{pp} \gamma^{1.28} (\gamma + 187.6)^{-0.2} + \Lambda_{io,p}, \quad (26)$$

with

$$\Lambda_{pp} \simeq 4.4 \cdot 10^{-16} \left( \frac{N_t}{\text{cm}^{-3}} \right) \text{s}^{-1}, \quad (27)$$

and

$$\Lambda_{io,p} \simeq 1.9 \cdot 10^{-16} \left( \frac{N_t}{\text{cm}^{-3}} \right) \text{s}^{-1}. \quad (28)$$

Note, that at energies  $\gamma \gg 1$  the ionization losses are negligible. Subsequently, the diffusion timescale (2) and the hadronic loss term (26) is used, so that the  $\zeta_0^p$ -term yields

$$\zeta_0^p(\gamma) = \ln \left( \Lambda_{pp} \gamma^{1.28} (\gamma + 187.6)^{-0.2} + \Lambda_{io} \right) - I_{diff}^p(\gamma), \quad (29)$$

with

$$\begin{aligned} I_{diff}^p(\gamma) &= \frac{cl_p}{R^2 \Lambda_{pp}} \int d\gamma \frac{\gamma^\beta}{\gamma^{1.28} (\gamma + 187.6)^{-0.2} + \frac{\Lambda_{io}}{\Lambda_{pp}}} \\ &\simeq \frac{cl_p}{R^2 \Lambda_{pp}} \frac{(\gamma + 187.6)^{0.2} \gamma^{\beta-0.28}}{(\beta - 0.28) (0.00533 \gamma + 1)^{0.2}} {}_2F_1(-0.2, \beta - 0.28; \beta + 0.72; -0.00533 \gamma). \end{aligned} \quad (30)$$

In the latter ionization losses are neglected and  ${}_2F_1(a, b; c; x)$  denotes the hypergeometric function. The source rate of relativistic protons is also determined by the accelerator, however, the continuous momentum losses of ultrarelativistic protons are too slow to have an effect on the accelerated energy spectrum. Hence, the source rate of the relativistic protons of Lorentz factor  $\gamma_{min} \leq \gamma \leq \gamma_{max}^p$  yields

$$q_p(\gamma) = q_0^p \gamma [\gamma^2 - 1]^{-\frac{\alpha+1}{2}} H[\gamma - \gamma_{min}] H[\gamma_{max}^p - \gamma]. \quad (31)$$

Consequently, with the loss term (26) and the eq. (29) the differential proton density yields

$$\begin{aligned} n_p(\gamma) = & q_0^p \left( \Lambda_{pp} \gamma^{1.28} (\gamma + 187.6)^{-0.2} + \Lambda_{io} \right)^{-1} \exp(F_{adv}^p(\gamma) + I_{diff}^p(\gamma)) \\ & \times \int_{\gamma_l}^{\gamma_{max}^p} d\gamma' \gamma' [\gamma'^2 - 1]^{-\frac{\alpha+1}{2}} \exp(-(F_{adv}^p(\gamma') + I_{diff}^p(\gamma'))), \end{aligned} \quad (32)$$

with

$$\begin{aligned} F_{adv}^p(\gamma) = & \int d\gamma [\tau_{adv} (\Lambda_{pp} \gamma^{1.28} (\gamma + 187.6)^{-0.2} + \Lambda_{io})]^{-1} \\ \simeq & -\frac{1}{\Lambda_{pp} \tau_{adv}} \frac{3.571 (\gamma + 187.6)^{0.2}}{(0.00533 \gamma + 1)^{0.2} \gamma^{0.28}} {}_2F_1(-0.28, -0.2; 0.72; -0.00533 \gamma). \end{aligned} \quad (33)$$

The lower integration limit is given by

$$\gamma_l = \begin{cases} \gamma, & \text{for } \gamma_{min} < \gamma < \gamma_{max}^p, \\ \gamma_{min}, & \text{for } \gamma \leq \gamma_{min}. \end{cases} \quad (34)$$

Here, the relativistic protons are supposed to have the same minimal Lorentz factor as the electrons, whereas the maximal Lorentz factor of the relativistic proton is constrained by the accelerator. Considering supernova remnants with a lifetime  $T_A \sim 1000$  yrs according to Gaisser (1990) we obtain  $\gamma_{max}^p = 10^{10} (B/1 \text{ G})$ .

### 2.3. Electron-to-Proton Ratio

If there exists a steady state description of relativistic electrons and protons within the starburst galaxy where no large scale electric fields occur (due to charge imbalance), the total number of injected relativistic electrons and protons will need to be the same. Hence, we demand

$$N_0 = T_A \int_{\gamma_0^e}^{\infty} d\gamma q_{e_1}(\gamma) = T_A \int_{\gamma_0^p}^{\infty} d\gamma q_p(\gamma) \quad (35)$$

where  $\gamma_0^{e,p}$  denotes the minimal Lorentz factor of relativistic protons and electrons, respectively. Usually,  $\gamma_0^{e,p} \simeq \left(\frac{10 \text{ keV}}{m_{e,p} c^2}\right) + 1$  is assumed (Schlickeiser (2001)) in order to consider electrons and protons above the non-relativistic kinetic energy of 10 keV. Since electrons and protons are supposed to be accelerated by the same cosmic accelerator, the lifetime  $T_A$  of the accelerator also needs to be the same.

Thus, the relation (35) enables to fix the  $q$ -ratio between the electron and proton source rate according to

$$\frac{q_0^e}{q_0^p} = \frac{[(\gamma_{max}^p)^2 - 1]^{-\frac{\alpha-1}{2}} - [(\gamma_0^p)^2 - 1]^{-\frac{\alpha-1}{2}}}{1 - \alpha} \left[ \int_{\gamma_0^e}^{\gamma_{max}^e} d\gamma \gamma [\gamma^2 - 1]^{-\frac{\alpha+1}{2}} (1 + A \gamma)^{-1} \right]^{-1}. \quad (36)$$

This ratio represents a generalization of previous results (e.g. Schlickeiser (2001), or Pohl (1993)) where in the case of an unbroken power-law distribution of electrons and protons a constant ratio of

$$\frac{q_0^e}{q_0^p} \simeq \left(\frac{m_p}{m_e}\right)^{(\alpha-1)/2} \quad (37)$$

is obtained. Note that it is more common to determine the ratio of the differential number of particles depend on its energy (or momentum) which results in the inverse of eq. (37).

### 3. Radio spectrum

The radio spectrum of starburst galaxies around a few GHz show a spectral index of about  $-0.5$  or steeper which is commonly explained by synchrotron radiation of relativistic electrons in the optically thin regime. However, most radio spectra flatten at smaller frequencies due to free-free absorption by the ionized gas within the starburst. In addition, the corresponding free-free emission can become dominant at the upper end of the radio spectrum which results in a flattening of the spectrum to a spectral index of about  $-0.1$  (Schlickeiser (2001)). Hence, the properties of the ionized gas needs to be taken into account in order to describe the influence of free-free radiation. But, to keep the number of free parameters as small as possible, we confine our model to the steep part of the radio spectrum between  $1 \text{ GHz} \lesssim \nu \lesssim 10 \text{ GHz}$  which needs to be dominated by synchrotron radiation. The influence of synchrotron self absorption is negligible, as free-free absorption dominates the spectrum in the optically thick regime below  $\sim 1 \text{ GHz}$ . The spectral synchrotron power is well described by

$$P_s(\nu, \gamma) = P_0 \left( \frac{\nu}{\nu_s \gamma^2} \right)^{1/3} \exp \left( \frac{\nu}{\nu_s \gamma^2} \right), \quad (38)$$

with  $P_0 = 2.65 \times 10^{-10} (B/1 \text{ G}) \text{ eV s}^{-1} \text{ Hz}^{-1}$  and a characteristic frequency  $\nu_s = 4.2 \times 10^6 (B/1 \text{ G}) \text{ Hz}$ . Hence, the isotropic, spontaneous synchrotron emission coefficient of the relativistic electron distribution (19) is given by

$$j_{syn}(\nu) = \frac{1}{4\pi} \int_1^\infty d\gamma n_e(\gamma) P_s(\nu, \gamma) = \frac{P_0}{4\pi} \left( \frac{\nu}{\nu_s} \right)^{\frac{1}{3}} \int_1^\infty d\gamma \gamma^{-\frac{2}{3}} \exp \left( \frac{\nu}{\nu_s \gamma^2} \right) n_e(\gamma) \quad (39)$$

The emergent synchrotron intensity (in units of  $\text{eV cm}^{-2} \text{ ster}^{-1} \text{ s}^{-1} \text{ Hz}^{-1}$ ) in the optically thin case is determined by  $I_{syn}(\nu, R) = j_{syn}(\nu) R$ , so that the corresponding synchrotron flux (in units of  $\text{eV cm}^{-2} \text{ s}^{-1} \text{ Hz}^{-1}$ ) at a distance  $d$  yields

$$\Phi_{syn}(\nu) = \frac{R^2}{d^2} 4\pi I_{syn}(\nu, R) = \frac{P_0 R^3}{d^2} \left( \frac{\nu}{\nu_s} \right)^{\frac{1}{3}} \int_1^\infty d\gamma \gamma^{-\frac{2}{3}} \exp \left( \frac{\nu}{\nu_s \gamma^2} \right) n_e(\gamma). \quad (40)$$

#### 4. Gamma radiation and secondary particles

Secondary particles are only generated by hadronic pion production, whereas, the gamma radiation results from non-thermal Bremsstrahlung, IC radiation and  $\pi^0$ – decay. However, the significance of each process depends pretty much on the magnetic field strength  $B$  and the target density  $N_t$ . Thereby, each process yields a certain source function  $q_i(E_i)$  of  $\gamma$ –rays ( $i = \gamma$ ) and secondaries ( $i = \{e, \nu_e, \nu_\mu\}$ ), respectively, in units of  $\text{cm}^{-3} \text{s}^{-1} \text{eV}^{-1}$ . Assuming the starburst galaxy to be opaque for  $\gamma$ –rays and neutrinos, the corresponding differential flux (in units of  $\text{cm}^{-2} \text{ster}^{-1} \text{s}^{-1} \text{eV}^{-1}$ ) at a distance  $d$  is determined by

$$\Phi_i(E_i) = \frac{R^2}{d^2} R q_i(E_i). \quad (41)$$

In the following, the source functions of each process are discussed in detail.

##### 4.1. Gamma radiation from non-thermal Bremsstrahlung

In addition to synchrotron radiation, the relativistic electrons are able to generate  $\gamma$ –rays by non-thermal Bremsstrahlung. According to Stecker (1971), the source function  $q_{\gamma,Br}(E_\gamma)$  for  $\gamma$ –rays (in units of  $\text{cm}^{-3} \text{s}^{-1} \text{eV}^{-1}$ ) is well approximated by

$$q_{\gamma,Br}(E_\gamma) = \frac{c N_t \sigma_{Br}}{E_\gamma} \int_{E_\gamma/(m_e c^2)}^{\infty} d\gamma n_e(\gamma), \quad (42)$$

where  $\sigma_{Br} \simeq 3.38 \cdot 10^{-26} \text{cm}^2$ .

##### 4.2. Gamma radiation from IC collisions

Another leptonic process that generates gamma-radiation is IC collisions of relativistic electrons with a photon field. In the case of starburst galaxies, the starlight that has been absorbed and re-radiated by dust in the infrared can be considered as the dominant photon field. Hence, the differential photon density  $n_{IR}(\epsilon)$  can be described by isotropic, diluted modified blackbody radiation according to the dust temperature  $T_d$  and the spatial dilution factor  $C_{dil}$ , so that

$$n_{IR}(\epsilon) = \frac{C_{dil}}{\pi^2 (\hbar c)^3} \frac{\epsilon^2}{\exp(\epsilon/(k_B T_d)) - 1} \left( \frac{\epsilon}{\epsilon_0} \right), \quad (43)$$

where  $T_d = 45 \text{K}$  and  $\epsilon_0 = 8.2 \text{meV}$  (Persic et al. (2008)). The referring energy density is given by  $U_{IR} = \int d\epsilon \epsilon n_{IR}(\epsilon) = 5.55 \cdot 10^{-8} C_{dil} \text{erg cm}^{-3}$ . Thus, the dilution factor  $C_{dil}$  is determined

by conversion to the observed energy density  $U_{IR} = 2.7 \cdot 10^{-10} L_{43} R_{200}^{-2} \text{ erg cm}^{-3}$ , which yields  $C_{dil} = 4.8 \cdot 10^{-3} L_{43} R_{200}^{-2}$ .

The resulting source function  $q_{\gamma, IC}(E_\gamma)$  for  $\gamma$ -rays is determined by (Rybicki and Lightman (1979))

$$q_{\gamma, IC}(E_\gamma) = \frac{3 c \sigma_T}{16 \pi} \int_0^\infty d\epsilon \frac{n_{IR}(\epsilon)}{\epsilon} \int_{\bar{\gamma}_{min}}^\infty d\gamma \frac{n_e(\gamma)}{\gamma^2} F(q, \Gamma), \quad (44)$$

where  $\sigma_T$  denotes the Thomson cross-section. The lower integration limit  $\bar{\gamma}_{min}$  is given by (Schlickeiser (2001))

$$\bar{\gamma}_{min} = \frac{E_\gamma}{2m_e c^2} \left[ 1 + \left( 1 + \frac{m_e^2 c^4}{\epsilon E_\gamma} \right)^{1/2} \right], \quad (45)$$

as well as the Klein-Nishina related function

$$F(q, \Gamma) = 2q \ln(q) + 1 + q - 2q^2 + \frac{(\Gamma q)^2 (1 - q)}{2(1 + \Gamma q)}, \quad (46)$$

where

$$\Gamma = \frac{4\epsilon\gamma}{m_e c^2} \quad \text{and} \quad q = \frac{E_\gamma}{\Gamma(\gamma m_e c^2 - E_\gamma)}. \quad (47)$$

### 4.3. Gamma radiation from $\pi^0$ -decay

The dominant gamma ray flux component in most starburst galaxies is supposed to be a result of the inelastic interactions of relativistic protons with the ambient medium due to hadronic pion production. Foremost, this interaction generates  $\pi^0$ -mesons which quasi-instantaneously decay into two gamma-rays. The corresponding energy spectra  $F_\gamma(x, E_p)$  of the resulting  $\gamma$ -rays with  $x = E_\gamma/E_p$  are given by Kelner et al. (2006). Using the relativistic proton density (32) in the relativistic limit where  $n_p(E_p) = n_p(\gamma = E_p/(m_p c^2))/(m_p c^2)$ , the gamma ray production rate is determined by

$$q_{\gamma, \pi^0}(E_\gamma) = c N_t \int_{E_\gamma}^\infty \frac{dE_p}{E_p} \sigma_{inel}(E_p) n_p(E_p) F_\gamma(x, E_p). \quad (48)$$

Here,  $\sigma_{inel}(E_p)$  denotes the inelastic part of the total cross-section of p-p interactions which is given by

$$\sigma_{inel}(E_p) = \begin{cases} (34.3 + 1.88 L + 0.25 L^2) \text{ mb}, & \text{for } E_p > 0.1 \text{ TeV}, \\ (34.3 + 1.88 L + 0.25 L^2) \cdot \left( 1 - \left( \frac{E_{th}}{E_p} \right)^4 \right)^2 \text{ mb}, & \text{for } E_{th} \leq E_p \leq 0.1 \text{ TeV}, \end{cases} \quad (49)$$

with  $L = \ln(E_p/1 \text{ TeV})$  and the threshold energy  $E_{th} = m_p c^2 + 2m_\pi c^2 + (m_\pi c^2)^2/(2m_p c^2)$  of the production of  $\pi^0$ -mesons.

#### 4.4. Neutrinos and secondary electrons from $\pi^\pm$ –decay

Additionally, hadronic pion production generates charged pions which quasi instantaneously decay according to  $\pi^\pm \rightarrow \mu^\pm + \nu_\mu(\bar{\nu}_\mu)$  and the generated muon decays on similar timescales in a 3-body process according to  $\mu^\pm \rightarrow e^\pm + \nu_e(\bar{\nu}_e) + \bar{\nu}_\mu(\nu_\mu)$ . Kelner et al. (2006) have also approximated the energy spectra of the resulting leptons. The total muon neutrino spectrum is determined by the sum of the first muon neutrino (directly from the pion) with an energy spectrum  $F_{\nu_\mu^{(1)}}(x, E_p)$  and the second muon neutrino (from the muon decay) corresponding to  $F_{\nu_\mu^{(2)}}(x, E_p)$ . The energy spectrum of the decay products of the muon are almost the same, so that i.e.  $F_{\nu_\mu^{(2)}}(x, E_p) \simeq F_{\nu_e}(x, E_p) \simeq F_e(x, E_p)$ .

Hence, the source function of muon and electron neutrinos is given by

$$q_{\nu_\mu}(E_\nu) = c N_t \int_{E_\nu}^{\infty} \frac{dE_p}{E_p} \sigma_{inel}(E_p) n_p(E_p) \left( F_{\nu_\mu^{(1)}}(x, E_p) + F_e(x, E_p) \right). \quad (50)$$

and

$$q_{\nu_e}(E_\nu) = c N_t \int_{E_\nu}^{\infty} \frac{dE_p}{E_p} \sigma_{inel}(E_p) n_p(E_p) F_e(x, E_p), \quad (51)$$

respectively, with the total inelastic cross-section  $\sigma_{inel}(E_p)$  according to eq. (49) and the dimensionless neutrino energy  $x = E_\nu/E_p$ .

In the relativistic limit, the (Lorentz factor dependent) source rate of secondary electrons that is needed in order to determine the relativistic electron density (19) is determined by

$$q_{e2}(\gamma) = q_{e2}(E_e) m_e c^2 = c N_t m_e c^2 \int_{E_e}^{\infty} \frac{dE_p}{E_p} \sigma_{inel}(E_p) n_p(E_p) F_e(x, E_p). \quad (52)$$

The fig. 3 shows that the significance of secondary electrons depends pretty much on the influence of IC losses on the primary electron spectrum according to  $A$ . For  $A < 10^{-5}$  the secondary electrons are negligible (i) in the case of target densities below a few hundred particles per cubic centimeter and (ii) when only the low energy part of the total source spectrum is considered.

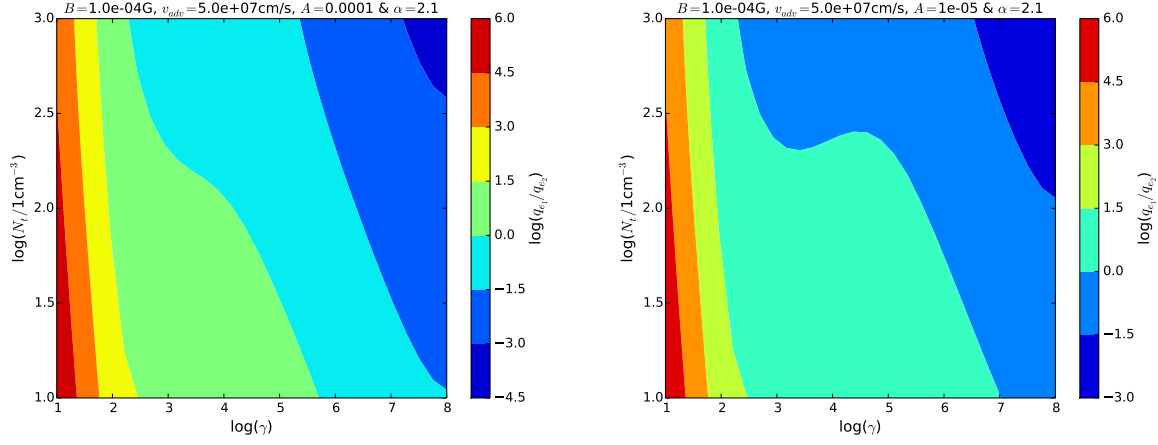


Fig. 3.—: Ratio of primary to secondary electrons for  $A = 10^{-4}$  (left) and  $A = 10^{-5}$  (right).

## 5. Consequences on the observations

The Fermi LAT 4-Year Point Source Catalog (3FGL) measured the gamma-ray flux of four different galaxies, namely NGC 253, M 82, NGC 4945 and NGC 1068. In addition, NGC 253 and M 82 have also been observed at TeV energies by the HESS and VERITAS telescopes, respectively. Here, the spectral shape does not change significantly, so that all four galaxies show a steep spectral behavior with a spectral index smaller than  $-2$ . In addition, all four starburst galaxies have been observed in the radio band with a spectral index smaller than  $-0.5$  between  $1.4 \text{ GHz} \leq \nu \lesssim 10 \text{ GHz}$ . NGC 253 and M 82 show a flattening of the spectrum at  $\nu \lesssim 1 \text{ GHz}$  which is supposed to refer to free-free absorption by a thermal gas. However, we do not account for this spectral behavior as it has already been shown (Yoast-Hull et al. (2014); Yoast-Hull et al. (2013)) that the free-free absorption of an additional warm ionized gas component is able to model the spectrum below 1 GHz. In contrast to the gamma-ray observations do the radio observations enable to resolve the sub-kpc structure of the starburst galaxies. Hence, there are radio observations of different spatial structures up to sub-arcsecond scales of the previously mentioned galaxies showing different flux behaviors. Especially the Seyfert 2 galaxies NGC 4945 and NGC 1068 show jet like structures that could be the driving force of the non-thermal emission. In general, the spatial boundary of the so-called starburst region is unclear, but as the gamma-ray flux on sub-arcsecond scales is unknown we need to consider the total radio flux of a few arcseconds. Therefore, we suppose the radio and gamma-ray flux from the innermost region of 400 pc of diameter, i.e.  $R_{200} = 1$  to be related to the starburst region. Furthermore, the relativistic particles are supposed to be homogeneously distributed in space which does not hold in the case of jet-driven emission. However, the effect of a complexer geometric structures as well as spatial inhomogeneities shall be addressed in future examinations.

In order to obtain the best-fit model we take into account that some data of different observations



indicate not to be in agreement with each other. In the case of the gamma-ray data, we exclude the last Fermi LAT data point within the fitting procedure, since TeV observations by VERITAS and HESS of M 82 and NGC 253, respectively, suggest the spectral behavior between 0.1 and 10 GeV to continue till a few TeV. In the case of the radio data, we exclude some observations due to computational limitations (in relation to the data by Williams and Bower (2010)) as well as discrepancies between different observations (in relation to NGC 253 and NGC 4945). Though all radio data show a range of agreement around a few GHz, so that the used data is chosen in order to obtain the most reasonable continuation to lower and higher frequencies.

The table 1 displays the distance  $d$  and the luminosity  $L_{IR} = 3.85 \cdot 10^{43} L_{43} \text{ erg s}^{-1}$  of the IR background between 8 and 1000  $\mu\text{m}$  which is related to the dominant photon field for IC interactions.

	NGC 253	M 82	NGC 4945	NGC 1068
$d$ [Mpc]	2.5	3.4	3.7	16.7
$L_{43}$	2.1	4.6	2.6	28

Table 1:: All data taken from Ackermann et al. (2012).

### 5.1. The best-fit model

In the following, the previously derived synchrotron and  $\gamma$ -ray flux are used to fit the radio and gamma data, respectively, in order to determine  $N_t$ ,  $B$ ,  $\alpha$ ,  $A$ ,  $q_0^{e,p}$ ,  $l_e$  and  $v_{adv}$  of the four starburst galaxies. Thereby, the ratio of the source rate  $q_0^e/q_0^p$  is already fixed by the quasi-neutrality of the source plasma according to eq. (36). In the case of  $N_t$ ,  $B$ ,  $\alpha$  and  $A$  we test 11250 ( $= 15 \times 15 \times 10 \times 5$ ) different value combinations within the reasonable parameter space of  $B = [10^{-4.5}; 10^{-3}] \text{ G}$ ,  $N_t = [10^{1.5}; 10^3] \text{ cm}^{-3}$ ,  $\alpha = [1.9; 2.4]$  and  $A = [10^{-4}; 10^{-8}]$ , respectively. Due to the computational intense calculations, we test our model only for  $l_e = \{10^{16}, 5 \cdot 10^{16}, 10^{17}, 5 \cdot 10^{17}\} \text{ cm}$  as well as  $v_{adv} = \{5 \cdot 10^7, 10^8, 5 \cdot 10^8\} \text{ cm/s}$ . The goodness of the fits is expressed by the sum of chi-squared test  $\chi_{radio}^2$  to the radio data and the chi-squared test  $\chi_\gamma^2$  to the gamma data. If several accurate fits to the data exist, we will apply a further condition to the best-fit model: We constrain the best-fit model by the resulting SN rate  $\nu_{SN}$ , although the correlation between the proton luminosity and  $\nu_{SN}$ , as given by eq. (53), has some uncertainties. When  $(\chi_{radio}^2 + \chi_\gamma^2)^{-1} \geq 0.13$ , we choose the best-fit to be the one with  $\nu_{SN}$  as close as possible to the expected value of around 0.2 SN per year (Torres and Reimer (2013)).

As shown in the Appendix B, the diffusion length  $l_e$  and  $l_p$ , respectively, has a bigger influence on the goodness of the fit than the galactic wind speed  $v_{adv}$ . However, the major influence is determined by the cooling parameters  $B$  and  $N_t$  as well as the initial source spectrum. The resulting best-fit model parameters of the individual starburst galaxies are displayed in table 2 and the corresponding radio and gamma flux is shown in fig. 4, respectively.

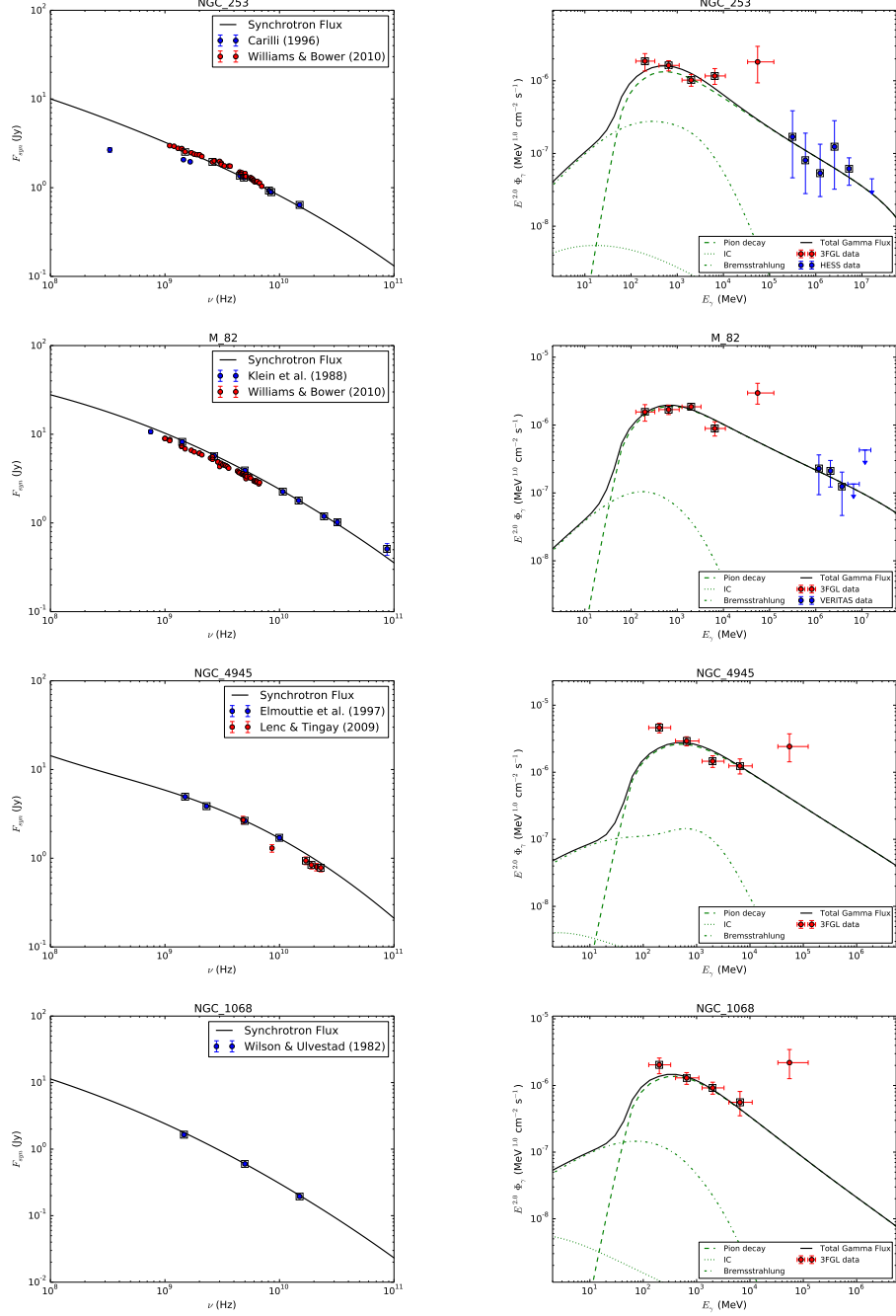


Fig. 4.—: The radio (left) and gamma-ray (right) data as well as the best-fit model of NGC 253, M 82, NGC 4945 and NGC 1068. Open squares represent the data set that is used for the  $\chi^2$  test.

	NGC 253	M 82	NGC 4945	NGC 1068
$q_0^e [10^{-18} \text{ cm}^{-3} \text{ s}^{-1}]$	1.5	1.0	9.3	208
$q_0^p [10^{-20} \text{ cm}^{-3} \text{ s}^{-1}]$	2.0	1.4	7.0	130
$\alpha$	2.15	2.15	2.3	2.35
$A$	$10^{-5}$	$10^{-4}$	$10^{-4}$	$10^{-4}$
$B [\mu\text{G}]$	109	611	178	178
$N_t [\text{cm}^{-3}]$	291	477	178	291
$v_{adv} [10^7 \text{ cm/s}]$	5	10	10	5
$l_e [10^{17} \text{ cm}]$	5	1	1	5
$q_{e1}/q_{e2} (\gamma = \sqrt{\nu_{GHz}/\nu_s})$	2.4 – 2.5	0.8 – 0.5	1.2 – 0.9	1.9 – 1.6
$\nu_{SN} [\text{yr}^{-1}]$	4	3	28	649

Table 2:: Best-fit model parameters

In the case of NGC 253 and M 82 the best-fit model describes the large data set of the radio and gamma-ray band very well. Also the best-fit model of NGC 1068 agrees very well with the data, however, the data set is much smaller. In the case of NGC 4945 the best-fit model describes the data the least good, which can be a result of the discrepancies of the radio data set.

Since most synchrotron radiation is emitted around the characteristic frequency  $\nu_s \gamma^2$ , we evaluate whether the radio flux at  $\nu_{GHz} = (1-10) \text{ GHz}$  is mostly produced by primary or secondary electrons. Hence, the ratio  $q_{e1}/q_{e2}$  at  $\gamma = \sqrt{\nu_{GHz}/\nu_s}$  for the best-fit model parameters is determined as displayed in table 2. For NGC 253 and NGC 1068 there is a slight dominance of primary electrons generating the observed synchrotron flux at a few GHz, whereas it is the opposite case for M 82. The radio flux of NGC 4945 is caused by primary and secondary electrons with almost the same fraction.

An important consequence on the particle acceleration process is given by the initial steepening of the electron distribution at  $\gamma_B \simeq A^{-1}$ . Here, the best-fit model indicates that the supposed influence of IC (or synchrotron) losses on a shock accelerated electron spectrum according to eq. (17) is in good agreement with the observations. Hence, we also approved that the common shock acceleration approach for a strong shock is at work when the diffusion coefficient in the accelerator and in the starburst region hardly deviate.

#### 5.1.1. Consequences on the supernova rate

When supernovae (SNe) represent the dominant source of relativistic protons, the initial proton source rate can be used to deduce the SN rate  $\nu_{SN}$  according to (e.g. Abdo et al. (2010))

$$\frac{4}{3} \pi R^3 \int_{\gamma_{min}}^{\gamma_{max}} d\gamma \gamma q_p(\gamma) = \nu_{SN} \frac{E_{SN}}{m_p c^2} \eta. \quad (53)$$

Here,  $E_{SN}$  denotes the kinetic energy released per SN and  $\eta$  is the acceleration efficiency of the relativistic protons. With a proton luminosity per SN of  $\eta E_{SN} = 10^{50}$  erg the resulting SN rate  $\nu_{SN}$  is determined (see table 2) using the best-fit model values of  $q_0^p$  and  $s$ . In general, the obtained rates  $\nu_{SN}$  are quite high, in particular in the case of NGC 4945 and NGC 1068. However, the SN rate decreases about an order of magnitude, when we suppose a high acceleration efficiency of relativistic protons, i.e.  $\eta \sim 1$ . Hence, the SN rate  $\nu_{SN}$  of M 82 and NGC 253 are in good agreement with previous results (Lacki et al. (2011)). For NGC 4945 and especially NGC 1068 we obtain  $\nu_{SN} \gg 1 \text{ yr}^{-1}$  even in the case of a high proton luminosity per SN. Thus, there needs to be an other relativistic proton source that dominates the acceleration of particles within NGC 4945 and NGC 1068. Here, the active galactic nucleus and the related jet-driven particle acceleration is a promising source candidate.

### 5.1.2. Consequences on the calorimetric behavior

Another important feature of starburst galaxies is their calorimetric behavior, i.e. whether or not the energy losses of cosmic-ray protons or electrons dominate over advection or diffusion losses. Hence, the best-fit model values of  $l_e$ ,  $v_{adv}$ ,  $B$  and  $N_t$  are used to determine the total energy loss timescale  $\tau_E^{e,p} = \gamma/|\dot{\gamma}|_{e,p}$  as well as the catastrophic loss timescales  $\tau_{adv}$  and  $\tau_{diff}$ . As shown in fig. 5 there is a crucial difference between the calorimetric behavior of relativistic protons and electrons. All considered starburst galaxies are a perfect electron calorimeter (with the exception of NGC 253 at a few GeV), whereas none of them is a proton calorimeter due to significant diffusion losses. However, the influence of the galactic wind on the relativistic protons only becomes significant in the case of M 82 and NGC 4945 at a few GeV. Thus, relativistic protons predominantly diffuse out of the starburst region following the magnetic field lines. In doing so, inelastic collisions generate secondary electrons which can form a synchrotron halo as observed in the case of M 82 (e.g. Reuter et al. (1992), Reuter et al. (1994)) and NGC 253 (e.g. Carilli et al. (1992)).

### 5.1.3. Consequences on the neutrino flux

A neutrino signal would be a clear indication of hadronic interactions within the starburst, however, no neutrino flux from these astrophysical sources has been observed so far. Therefore, it is useful to determine the expected neutrino flux of the considered starburst galaxies based on the observed gamma-ray flux. In doing so, the best-fit model parameters of table 2 are used to determine the resulting neutrino flux. Fig. 6 shows that NGC 253, M 82, NGC 4945 and NGC 1068 are potential sources for high energy neutrinos. However, the neutrino flux of all four starburst galaxies is below the current observation limit of the *IceCube* neutrino detector.

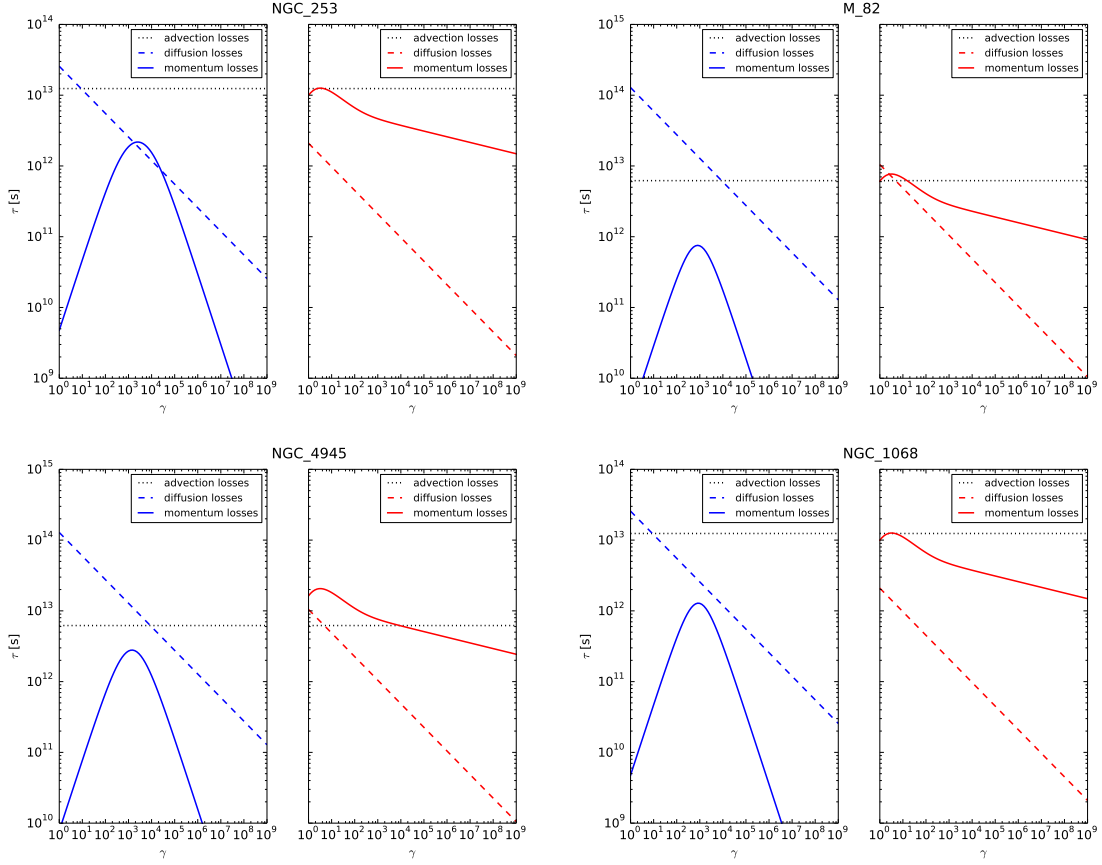


Fig. 5.—: The resulting loss timescales of electrons (blue) and protons (red) of NGC 253, M 82, NGC 4945 and NGC 1068 that correspond to the best-fit model parameters.

## 6. Conclusions

The present paper examines the radiation processes in starburst galaxies. In doing so, a steady state description of the relativistic particles within the spherically symmetric inner hundreds of parsecs of the galaxy is used. We suppose homogeneously distributed sources of relativistic particles that generate a power-law distribution between a minimal and a maximal momentum. Due to the strong cooling of the ultrarelativistic electrons (via IC or synchrotron losses) the electron source rate can steepen at a Lorentz factor  $\gamma_B = 1/A$  by one. A general solution of the relativistic particle distribution is given and subsequently specified by the particle dependent source rate, cooling mechanism and diffusion loss rate. In doing so, we emphasize the significance of diffusion losses over advection losses, especially in the case of the relativistic protons.

There is a strong evidence of negligible electric fields on large scales within starburst galaxies, so that the source of the relativistic plasma of electrons and protons needs to be quasi-neutral. Due to the broken power law distribution of the electron source rate, the source rate ratio  $q_0^e/q_0^p$  increases

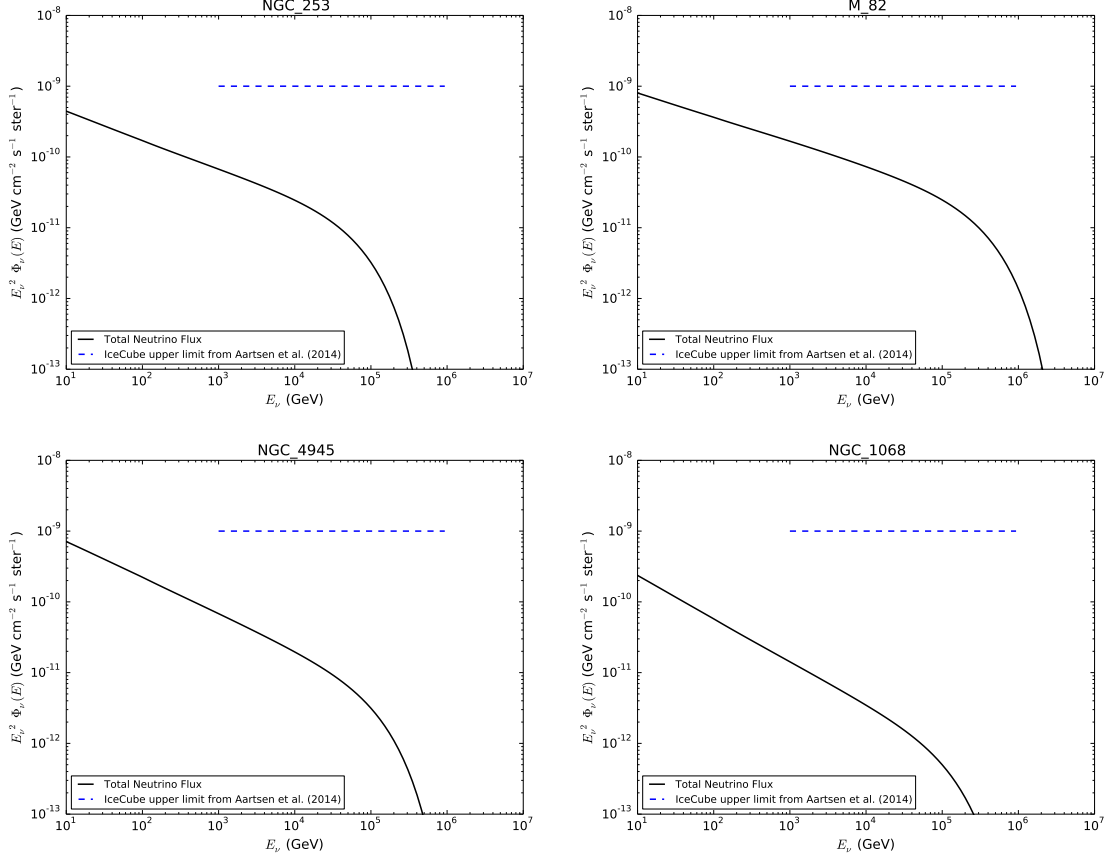


Fig. 6.—: The differential neutrino flux of NGC 253, M 82, NGC 4945 and NGC 1068 that results from the best-fit model parameters. The blue dashed lines represent IceCube limits for the specific source from Aartsen et al. (2014).

with decreasing  $\gamma_B$  and can become much bigger than the commonly used ratio of  $(m_p/m_e)^{(\alpha-1)/2}$ . Using the primary electrons from the accelerator as well as the secondary electrons from hadronic pion production, we determine the resulting synchrotron radiation as well as the gamma radiation by Bremsstrahlung and IC collisions of the relativistic electrons. However, the main constituent of the gamma ray flux of starburst galaxies is given by the gamma radiation from hadronic pion production of the relativistic protons as shown in Section 5. In addition, we account for secondary electrons and neutrinos that are generated by the decay of charged pions.

Finally, we tested 135000 ( $= 15 \times 15 \times 10 \times 5 \times 4 \times 3$ ) different combinations within a reasonable parameter range of  $(B, N_t, \alpha, A, l_e, v_{adv})$  in order to obtain the best-fit model parameters of four different starburst galaxies which are summarized in table 2. As shown in fig. 4, the radio and gamma-ray flux of our best-fit model is in very good agreement with the observations of M 82, NGC 253 and NGC 1068, whereas in the case of NGC 4945 our best-fit model slightly deviates from the observed flux at  $(0.1 - 0.3)$  GeV and  $\sim 20$  GHz.

In order to explain the observed radio flux we expose that primary and secondary electrons are needed. However, in the case of NGC 253 and NGC 1068 the synchrotron flux around a few GHz is slightly dominated by the primary electrons, whereas the secondary electrons slightly dominate in the case of M 82.

Furthermore, the best-fit model indicates, that there is a significant influence of IC (or synchrotron) losses on the initial shock accelerated electron spectrum at energies  $> 5$  GeV (for M 82, NGC 4945, NGC 1068) and  $> 50$  GeV (for NGC 253), respectively.

Using the best-fit model parameter values of  $q_0^p$  and  $\alpha$  we determine the SN rate  $\nu_{SN}$  based on a proton luminosity per SN of  $\eta E_{SN} = 10^{50}$  erg. For M 82 and NGC 253 we obtain a reasonable rate of  $\nu_{SN} \sim 1 \text{ yr}^{-1}$ , whereas the Seyfert 2 galaxies NGC 4945 and NGC 1068 yield a SN rate of  $\nu_{SN} \gg 1 \text{ yr}^{-1}$ . Hence, other particle accelerators (e.g. the active galactic nucleus) within NGC 4945 and NGC 1068 need to be at work, since the origin of the relativistic particles cannot be dominated by SNe.

In addition, we reveal that the four starburst galaxies are perfect electron calorimeters (with the exception of NGC 253 at a few GeV). However, there is a significant loss of relativistic protons due to diffusion (see fig. 5). Thus, the observed synchrotron halos of M 82 and NGC 253 need to be a consequence of the secondary electrons generated by the relativistic protons that diffuse out of the starburst region.

Finally, it is shown (see fig. 6) that NGC 253, M 82, NGC 4945 and NGC 1068 are potential high energy neutrino sources, however, the expected neutrino flux is below current observation limits.

We are grateful to Dominik Elsässer, Reinhard Schlickeiser, Ralf-Jürgen Dettmar, Sebastian Schöneberg, Florian Schuppan and Lukas Merten for very useful comments and suggestions that helped to improve the original version of the paper. We acknowledge support from the DFG Research group FOR 1048 on “Instabilities, Turbulence and Transport in Cosmic Magnetic Fields” (project BE 3714/5-1) as well as from the MERCUR project St-2014-0040 (RAPP center) and the research department of plasmas with complex interactions (Bochum).

## A. General solution of the steady state particle transport equation

In order to solve the transport equation (1) we substitute

$$n_{e,p}(\gamma) = \tilde{n}_{e,p}(\gamma) \exp \left( \int \frac{d\gamma}{|\dot{\gamma}|_{e,p} \tau_{adv}} \right) \quad (\text{A1})$$

so that

$$0 = \frac{\partial}{\partial \gamma} (|\dot{\gamma}|_{e,p} \tilde{n}_{e,p}) - \frac{\tilde{n}_{e,p}}{\tau_{diff}^{e,p}(\gamma)} + \tilde{q}_{e,p}(\gamma), \quad (\text{A2})$$

with

$$\tilde{q}_{e,p}(\gamma) = q_{e,p}(\gamma) \exp \left( - \int \frac{d\gamma}{|\dot{\gamma}|_{e,p} \tau_{adv}} \right). \quad (\text{A3})$$

For non-vanishing continuous energy losses, the transport Eq. (A2) can easily be rearranged to

$$0 = \frac{\partial \tilde{n}_{e,p}}{\partial \gamma} + \left( \frac{1}{|\dot{\gamma}|} \frac{\partial |\dot{\gamma}|}{\partial \gamma} - \frac{1}{\tau_{diff}(\gamma) |\dot{\gamma}|} \right) \tilde{n}_{e,p}(\gamma) + \frac{\tilde{q}_{e,p}(\gamma)}{|\dot{\gamma}'|}. \quad (\text{A4})$$

Using the method of variation of a constant the previous equation is solved by

$$\tilde{n}_{e,p}(\gamma) = n_0^{e,p} \exp(-\zeta_0^{e,p}(\gamma)) \left( 1 - \frac{1}{n_0^{e,p} \zeta_1^{e,p}(\gamma)} \right), \quad (\text{A5})$$

where

$$\zeta_0^{e,p}(\gamma) = \int d\gamma \frac{1}{|\dot{\gamma}|_{e,p}} \frac{\partial |\dot{\gamma}|_{e,p}}{\partial \gamma} - \frac{1}{\tau_{diff}^{e,p}(\gamma) |\dot{\gamma}|_{e,p}} \quad (\text{A6})$$

and

$$\zeta_1(\gamma) = \int_{\gamma_0}^{\gamma} d\gamma' \frac{\tilde{q}_{e,p}(\gamma')}{|\dot{\gamma}'|_{e,p}} \exp(\zeta_0^{e,p}(\gamma')). \quad (\text{A7})$$

With eq. (A1) the relativistic particle density is generally given by

$$n_{e,p}(\gamma) = n_0^{e,p} \exp \left( \int \frac{d\gamma}{|\dot{\gamma}|_{e,p} \tau_{adv}} \right) \exp(-\zeta_0^{e,p}(\gamma)) \left( 1 - \frac{1}{n_0^{e,p} \zeta_1^{e,p}(\gamma)} \right), \quad (\text{A8})$$

In order to determine the constants  $n_0^{e,p}$  and  $\gamma_0$  we need appropriate boundary conditions. The first condition (i) demands a vanishing particle density when there is no source rate, i.e.  $n_{e,p}(\gamma) = 0$  for  $q_{e,p}(\gamma) = 0$ . Consequently,  $n_0^{e,p} = 0$  so that the solution (A8) simplifies to

$$n_{e,p}(\gamma) = - \exp \left( \int \frac{d\gamma}{|\dot{\gamma}|_{e,p} \tau_{adv}} \right) \exp(-\zeta_0^{e,p}(\gamma)) \zeta_1^{e,p}(\gamma). \quad (\text{A9})$$

The second condition (ii) demands that there is a maximum particle Lorentz factor given by  $q_{e,p}(\gamma) = f(\gamma) H[\gamma_{max} - \gamma]$ . Thus,  $n_{e,p}(\gamma \geq \gamma_{max}) = 0$  yields that  $\gamma_0 = \gamma_{max}$ , so that the differential particle density (A9) yields

$$n_{e,p}(\gamma) = \exp \left( \int \frac{d\gamma}{|\dot{\gamma}|_{e,p} \tau_{adv}} \right) e^{-\zeta_0^{e,p}(\gamma)} \int_{\gamma}^{\gamma_{max}} d\gamma' \frac{q_{e,p}(\gamma')}{|\dot{\gamma}'|_{e,p}} e^{\zeta_0^{e,p}(\gamma')} \exp \left( - \int \frac{d\gamma'}{|\dot{\gamma}'|_{e,p} \tau_{adv}} \right). \quad (\text{A10})$$

## B. Generation of a best-fit model

Using a selection of the observations in the radio and gamma-ray band (as displayed in fig. 4), we calculate the chi-squared tests  $\chi_{radio}^2$  and  $\chi_{\gamma}^2$  according to the radio and gamma-ray data, respectively. First, we choose a certain mean free path  $l_e$  and  $l_p$ , respectively, as well as a galactic wind speed  $v_{adv}$  and determine  $\chi_{radio}^2$  and  $\chi_{\gamma}^2$  in the whole parameter space of  $(N_t, B, \alpha, A)$ . Hence,  $\chi_{radio}^2$  and  $\chi_{\gamma}^2$  for 11250 ( $= 15 \times 15 \times 10 \times 5$ ) different parameter sets are evaluated and the total maximum of  $(\chi_{radio}^2 + \chi_{\gamma}^2)^{-1}$  is determined. Afterward, the same procedure is done for eleven other parameters sets of  $(l_e, v_{adv})$ .



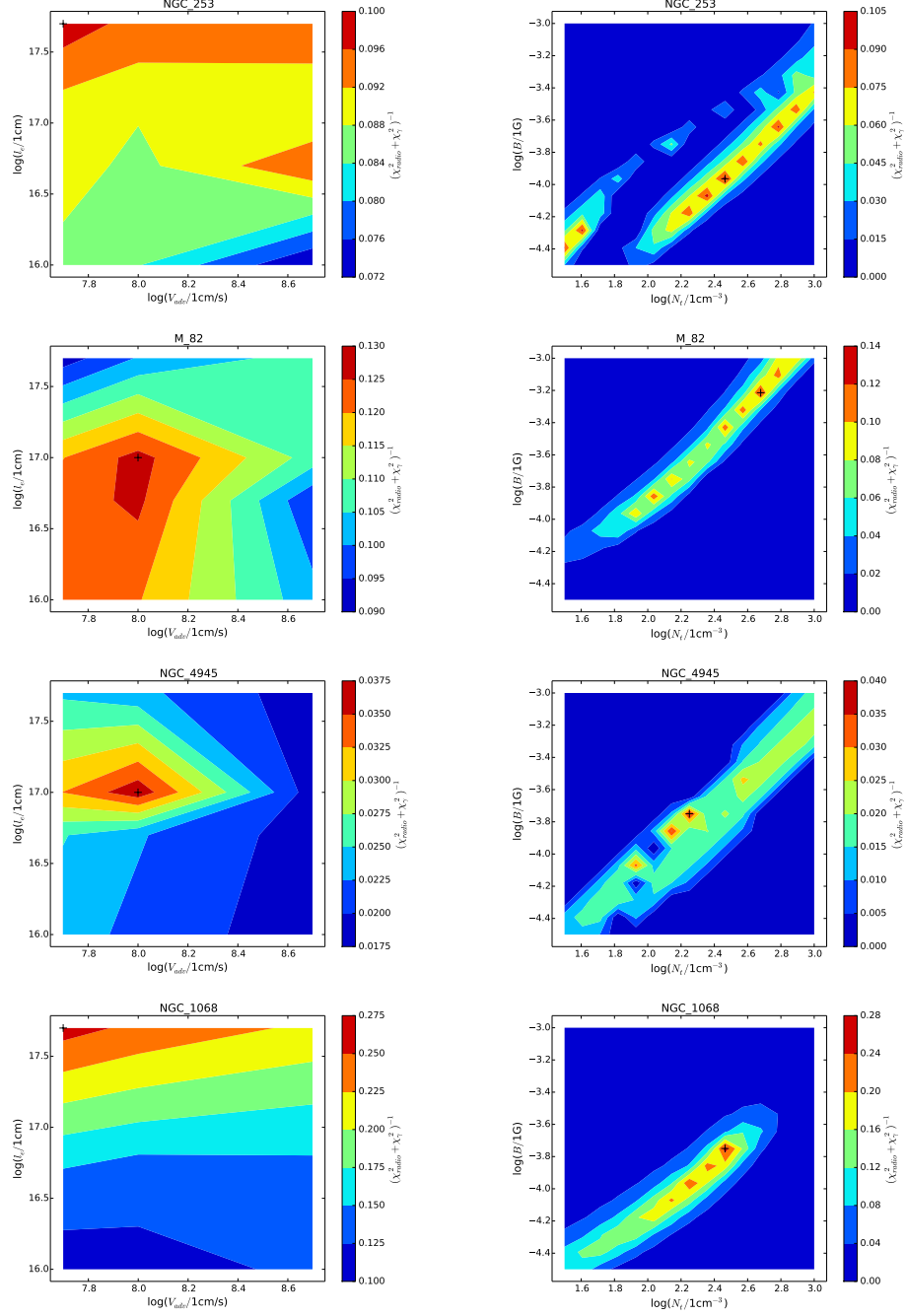


Fig. 7.— The inverse sum of the chi-squared test to the radio and gamma-ray data dependent on  $l_e$  and  $v_{adv}$  (left) as well as  $B$  and  $N_t$  (right) of NGC 253, M 82, NGC 4945 and NGC 1068. The black cross marks the best-fit model parameter values.

The resulting maximum of  $(\chi_{radio}^2 + \chi_{\gamma}^2)^{-1}$  dependent on  $l_e$  and  $v_{adv}$  (as displayed on the left hand side of fig. 7) yields the best-fit model parameters of  $l_e$  ( $l_p$ ) and  $v_{adv}$  for each starburst galaxy. However, in the case of multiple fits with  $(\chi_{radio}^2 + \chi_{\gamma}^2)^{-1} \geq 0.13$ , the best-fit model is the one where the difference between the resulting SN rate  $\nu_{SN}$  and the expected rate of 0.2 SN per year (Torres and Reimer (2013)) is minimal. The right hand side of fig. 7 shows the values of  $(\chi_{radio}^2 + \chi_{\gamma}^2)^{-1}$  dependent on  $N_t$  and  $B$  that correspond to the best-fit model values of the mean free path and the galactic wind speed.

## REFERENCES

- M. G. Aartsen, M. Ackermann, J. Adams, J. A. Aguilar, M. Ahlers, M. Ahrens, D. Altmann, T. Anderson, C. Argüelles, T. C. Arlen, and et al. Searches for Extended and Point-like Neutrino Sources with Four Years of IceCube Data. *ApJ*, 796:109, December 2014.
- A. A. Abdo, M. Ackermann, M. Ajello, W. B. Atwood, M. Axelsson, L. Baldini, J. Ballet, G. Barbiellini, D. Bastieri, K. Bechtol, R. Bellazzini, B. Berenji, E. D. Bloom, E. Bonamente, A. W. Borgland, J. Bregeon, A. Brez, M. Brigida, P. Bruel, T. H. Burnett, G. A. Calian-dro, R. A. Cameron, P. A. Caraveo, J. M. Casandjian, E. Cavazzuti, C. Cecchi, Ö. Çelik, E. Charles, A. Chekhtman, C. C. Cheung, J. Chiang, S. Ciprini, R. Claus, J. Cohen-Tanugi, J. Conrad, C. D. Dermer, A. de Angelis, F. de Palma, S. W. Digel, E. d. C. e. Silva, P. S. Drell, A. Drlica-Wagner, R. Dubois, D. Dumora, C. Farnier, C. Favuzzi, S. J. Fegan, W. B. Focke, L. Foschini, M. Frailis, Y. Fukazawa, S. Funk, P. Fusco, F. Gargano, D. Gasparrini, N. Gehrels, S. Germani, B. Giebels, N. Giglietto, F. Giordano, T. Glanzman, G. Godfrey, I. A. Grenier, M.-H. Grondin, J. E. Grove, L. Guillemot, S. Guiriec, Y. Hanabata, A. K. Harding, M. Hayashida, E. Hays, R. E. Hughes, G. Jóhannesson, A. S. Johnson, R. P. Johnson, W. N. Johnson, T. Kamae, H. Katagiri, J. Kataoka, N. Kawai, M. Kerr, J. Knödseder, M. L. Kocian, M. Kuss, J. Lande, L. Latronico, M. Lemoine-Goumard, F. Longo, F. Loparco, B. Lott, M. N. Lovellette, P. Lubrano, G. M. Madejski, A. Makeev, M. N. Mazziotta, W. McConville, J. E. McEnery, C. Meurer, P. F. Michelson, W. Mitthumsiri, T. Mizuno, A. A. Moiseev, C. Monte, M. E. Monzani, A. Morselli, I. V. Moskalenko, S. Murgia, T. Nakamori, P. L. Nolan, J. P. Norris, E. Nuss, T. Ohsugi, N. Omodei, E. Orlando, J. F. Ormes, M. Ozaki, D. Paneque, J. H. Panetta, D. Parent, V. Pelassa, M. Pepe, M. Pesce-Rollins, F. Piron, T. A. Porter, S. Rainò, R. Rando, M. Razzano, A. Reimer, O. Reimer, T. Reposeur, S. Ritz, A. Y. Rodriguez, R. W. Romani, M. Roth, F. Ryde, H. F.-W. Sadrozinski, A. Sander, P. M. Saz Parkinson, J. D. Scargle, A. Sellerholm, C. Sgrò, M. S. Shaw, D. A. Smith, P. D. Smith, G. Spandre, P. Spinelli, M. S. Strickman, A. W. Strong, D. J. Suson, H. Takahashi, T. Tanaka, J. B. Thayer, J. G. Thayer, D. J. Thompson, L. Tibaldo, O. Tibolla, D. F. Torres, G. Tosti, A. Tramacere, Y. Uchiyama, T. L. Usher, V. Vasileiou, N. Vilchez, V. Vitale, A. P. Waite, P. Wang, B. L. Winer, K. S. Wood, T. Ylinen, M. Ziegler, and Fermi LAT

- Collaboration. Detection of Gamma-Ray Emission from the Starburst Galaxies M82 and NGC 253 with the Large Area Telescope on Fermi. *ApJ*, 709:L152–L157, February 2010.
- A. Abramowski, F. Acero, F. Aharonian, A. G. Akhperjanian, G. Anton, A. Balzer, A. Barnacka, Y. Becherini, J. Becker, K. Bernlöhner, E. Birsin, J. Biteau, A. Bochow, C. Boisson, J. Bolmont, P. Bordas, J. Brucker, F. Brun, P. Brun, T. Bulik, I. Büsching, S. Carrigan, S. Casanova, M. Cerruti, P. M. Chadwick, A. Charbonnier, R. C. G. Chaves, A. Cheesebrough, G. Cologna, J. Conrad, C. Couturier, M. Dalton, M. K. Daniel, I. D. Davids, B. Degrange, C. Deil, H. J. Dickinson, A. Djannati-Ataï, W. Domainko, L. O. Drury, G. Dubus, K. Dutson, J. Dyks, M. Dyrda, K. Egberts, P. Eger, P. Espigat, L. Fallon, S. Fegan, F. Feinstein, M. V. Fernandes, A. Fiasson, G. Fontaine, A. Förster, M. Füßling, M. Gajdus, Y. A. Gallant, T. Garrigoux, H. Gast, L. Gérard, B. Giebels, J. F. Glicenstein, B. Glück, D. Göring, M.-H. Grondin, S. Häffner, J. D. Hague, J. Hahn, D. Hampf, J. Harris, M. Hauser, S. Heinz, G. Heinzelmann, G. Henri, G. Hermann, A. Hillert, J. A. Hinton, W. Hofmann, P. Hofverberg, M. Holler, D. Horns, A. Jacholkowska, C. Jahn, M. Jamroz, I. Jung, M. A. Kastendieck, K. Katarzyński, U. Katz, S. Kaufmann, B. Khélifi, D. Klockov, W. Kluźniak, T. Kneiske, N. Komin, K. Kosack, R. Kossakowski, F. Krayzel, H. Laffon, G. Lamanna, J.-P. Lenain, D. Lennarz, T. Lohse, A. Lopatin, C.-C. Lu, V. Marandon, A. Marcowith, J. Masbou, G. Maurin, N. Maxted, M. Mayer, T. J. L. McComb, M. C. Medina, J. Méhault, R. Moderski, M. Mohamed, E. Moulin, C. L. Naumann, M. Naumann-Godo, M. de Naurois, D. Nedbal, D. Nekrassov, N. Nguyen, B. Nicholas, J. Niemiec, S. J. Nolan, S. Ohm, E. de Oña Wilhelmi, B. Opitz, M. Ostrowski, I. Oya, M. Panter, M. Paz Arribas, N. W. Pekeur, G. Pelletier, J. Perez, P.-O. Petrucci, B. Peyaud, S. Pita, G. Pühlhofer, M. Punch, A. Quirrenbach, M. Raue, A. Reimer, O. Reimer, M. Renaud, R. de los Reyes, F. Rieger, J. Ripken, L. Rob, S. Rosier-Lees, G. Rowell, B. Rudak, C. B. Rulten, V. Sahakian, D. A. Sanchez, A. Santangelo, R. Schlickeiser, A. Schulz, U. Schwanke, S. Schwarzbach, S. Schwemmer, F. Sheidaei, J. L. Skilton, H. Sol, G. Spengler, L. Stawarz, R. Steenkamp, C. Stegmann, F. Stinzing, K. Stycz, I. Sushch, A. Szostek, J.-P. Tavernet, R. Terrier, M. Tluczykont, K. Valerius, C. van Eldik, G. Vasileiadis, C. Venter, A. Viana, P. Vincent, H. J. Völk, F. Volpe, S. Vorobiov, M. Vorster, S. J. Wagner, M. Ward, R. White, A. Wiercholska, M. Zacharias, A. Zajczyk, A. A. Zdziarski, A. Zech, H.-S. Zechlin, and H. E. S. S. Collaboration. Spectral Analysis and Interpretation of the  $\gamma$ -Ray Emission from the Starburst Galaxy NGC 253. *ApJ*, 757:158, October 2012.
- M. Ackermann, M. Ajello, A. Allafort, L. Baldini, J. Ballet, D. Bastieri, K. Bechtol, R. Bellazzini, B. Berenji, E. D. Bloom, E. Bonamente, A. W. Borgland, A. Bouvier, J. Bregeon, M. Brigida, P. Bruel, R. Buehler, S. Buson, G. A. Caliandro, R. A. Cameron, P. A. Caraveo, J. M. Casandjian, C. Cecchi, E. Charles, A. Chekhtman, C. C. Cheung, J. Chiang, A. N. Cillis, S. Ciprini, R. Claus, J. Cohen-Tanugi, J. Conrad, S. Cutini, F. de Palma, C. D. Dermer, S. W. Digel, E. d. C. e. Silva, P. S. Drell, A. Drlica-Wagner, C. Favuzzi, S. J. Fegan, P. Fortin, Y. Fukazawa, S. Funk, P. Fusco, F. Gargano, D. Gasparrini, S. Germani, N. Giglietto,

- F. Giordano, T. Glanzman, G. Godfrey, I. A. Grenier, S. Guiriec, M. Gustafsson, D. Hadasch, M. Hayashida, E. Hays, R. E. Hughes, G. Jóhannesson, A. S. Johnson, T. Kamae, H. Kata-giri, J. Kataoka, J. Knödseder, M. Kuss, J. Lande, F. Longo, F. Loparco, B. Lott, M. N. Lovellette, P. Lubrano, G. M. Madejski, P. Martin, M. N. Mazziotta, J. E. McEnery, P. F. Michelson, T. Mizuno, C. Monte, M. E. Monzani, A. Morselli, I. V. Moskalenko, S. Murgia, S. Nishino, J. P. Norris, E. Nuss, M. Ohno, T. Ohsugi, A. Okumura, N. Omodei, E. Orlando, M. Ozaki, D. Parent, M. Persic, M. Pesce-Rollins, V. Petrosian, M. Pierbattista, F. Piron, G. Pivato, T. A. Porter, S. Rainò, R. Rando, M. Razzano, A. Reimer, O. Reimer, S. Ritz, M. Roth, C. Sbarra, C. Sgrò, E. J. Siskind, G. Spandre, P. Spinelli, L. Stawarz, A. W. Strong, H. Takahashi, T. Tanaka, J. B. Thayer, L. Tibaldo, M. Tinivella, D. F. Torres, G. Tosti, E. Troja, Y. Uchiyama, J. Vandenbroucke, G. Vianello, V. Vitale, A. P. Waite, M. Wood, and Z. Yang. GeV Observations of Star-forming Galaxies with the Fermi Large Area Telescope. *ApJ*, 755:164, August 2012.
- J. Becker Tjus, B. Eichmann, F. Halzen, A. Kheirandish, and S. M. Saba. High-energy neutrinos from radio galaxies. *Phys. Rev. D*, 89(12):123005, June 2014.
- V. S. Berezinskii, S. V. Bulanov, V. A. Dogiel, and V. S. Ptuskin. *Astrophysics of cosmic rays*. 1990.
- C. L. Carilli. Free-free absorption towards the nucleus of NGC 253: further evidence for high pressures in the starburst nucleus. *A&A*, 305:402, January 1996.
- C. L. Carilli, M. A. Holdaway, P. T. P. Ho, and C. G. de Pree. Discovery of a synchrotron-emitting halo around NGC 253. *ApJ*, 399:L59–L62, November 1992.
- C. D. Dermer and G. Menon. *High Energy Radiation from Black Holes: Gamma Rays, Cosmic Rays, and Neutrinos*. 2009.
- M. Elmouttie, R. F. Haynes, K. L. Jones, M. Ehle, R. Beck, J. I. Harnett, and R. Wielebinski. The radio continuum structure of the edge-on spiral galaxy NGC 4945. *MNRAS*, 284:830–838, February 1997.
- T. K. Gaisser. *Cosmic rays and particle physics*. 1990.
- J. F. Gallimore, S. A. Baum, and C. P. O’Dea. The Subarcsecond Radio Structure in NGC 1068. II. Implications for the Central Engine and Unifying Schemes. *ApJ*, 464:198, June 1996.
- V. Heesen, R. Beck, M. Krause, and R.-J. Dettmar. Cosmic rays and the magnetic field in the nearby starburst galaxy NGC 253. I. The distribution and transport of cosmic rays. *A&A*, 494:563–577, February 2009.
- G. Helou, B. T. Soifer, and M. Rowan-Robinson. Thermal infrared and nonthermal radio - Remarkable correlation in disks of galaxies. *ApJ*, 298:L7–L11, November 1985.

- D. Hooper, P. Blasi, and P. Dario Serpico. Pulsars as the sources of high energy cosmic ray positrons. *J. Cosmology Astropart. Phys.*, 1:25, January 2009.
- S. R. Kelner, F. A. Aharonian, and V. V. Bugayov. Energy spectra of gamma rays, electrons, and neutrinos produced at proton-proton interactions in the very high energy regime. *Phys. Rev. D*, 74(3):034018, August 2006.
- U. Klein, R. Wielebinski, and H. W. Morsi. Radio continuum observations of M82. *A&A*, 190:41–46, January 1988.
- S. Krakau and R. Schlickeiser. Pion Production Momentum Loss of Cosmic Ray Hadrons. *ApJ*, 802:114, April 2015.
- B. C. Lacki, T. A. Thompson, E. Quataert, A. Loeb, and E. Waxman. On the GeV and TeV Detections of the Starburst Galaxies M82 and NGC 253. *ApJ*, 734:107, June 2011.
- J.-P. Lenain, C. Ricci, M. Türler, D. Dorner, and R. Walter. Seyfert 2 galaxies in the GeV band: jets and starburst. *A&A*, 524:A72, December 2010.
- K. Mannheim, D. Elsässer, and O. Tibolla. Gamma-rays from pulsar wind nebulae in starburst galaxies. *Astroparticle Physics*, 35:797–800, July 2012.
- K. Mannheim and R. Schlickeiser. Interactions of cosmic ray nuclei. *A&A*, 286:983–996, June 1994.
- S. Ohm and J. A. Hinton. Non-thermal emission from pulsar-wind nebulae in starburst galaxies. *MNRAS*, 429:L70–L74, February 2013.
- T. A. D. Paglione and R. D. Abrahams. Properties of nearby Starburst Galaxies Based on their Diffuse Gamma-Ray Emission. *ApJ*, 755:106, August 2012.
- J. Park, D. Caprioli, and A. Spitkovsky. Simultaneous Acceleration of Protons and Electrons at Nonrelativistic Quasiparallel Collisionless Shocks. *Physical Review Letters*, 114(8):085003, February 2015.
- M. Persic, Y. Rephaeli, and Y. Arieli. Very-high-energy emission from M 82. *A&A*, 486:143–149, July 2008.
- M. Pohl. On the predictive power of the minimum energy condition. I - Isotropic steady-state configurations. *A&A*, 270:91–101, March 1993.
- G. W. Prölss and M. K. Bird. *Physics of the Earth’s Space Environment: an introduction*. Springer-Verlag Berlin Heidelberg, 2004.
- H.-P. Reuter, U. Klein, H. Lesch, R. Wielebinski, and P. P. Kronberg. Gaps and filaments in the synchrotron halo of M82 - Evidence for poloidal magnetic fields. *A&A*, 256:10–18, March 1992.

- H.-P. Reuter, U. Klein, H. Lesch, R. Wielebinski, and P. P. Kronberg. The magnetic field in the halo of M 82. Polarized radio emission at  $\lambda\lambda(6.2)$  and 3.6 CM. *A&A*, 282:724–730, February 1994.
- G. B. Rybicki and A. P. Lightman. *Radiative processes in astrophysics*. 1979.
- R. Schlickeiser. *Cosmic Ray Astrophysics*. 2002.
- P. L. Shopbell and J. Bland-Hawthorn. The Asymmetric Wind in M82. *ApJ*, 493:129–153, January 1998.
- F. W. Stecker. Cosmic gamma rays. *NASA Special Publication*, 249, 1971.
- F. W. Stecker. Are diffuse high energy neutrinos and  $\gamma$ -rays from starburst galaxies observable? *Astroparticle Physics*, 26:398–401, January 2007.
- I. R. Stevens, A. M. Read, and J. Bravo-Guerrero. First-look XMM-Newton EPIC observations of the prototypical starburst galaxy M82. *MNRAS*, 343:L47–L52, August 2003.
- C. M. Telesco and D. A. Harper. Galaxies and far-infrared emission. *ApJ*, 235:392–404, January 1980.
- D. F. Torres and O. Reimer, editors. *Cosmic Rays in Star-Forming Environments*, volume 34 of *Astrophysics and Space Science Proceedings*, 2013.
- VERITAS Collaboration, V. A. Acciari, E. Aliu, T. Arlen, T. Aune, M. Bautista, M. Beilicke, W. Benbow, D. Boltuch, S. M. Bradbury, J. H. Buckley, V. Bugaev, K. Byrum, A. Cannon, O. Celik, A. Cesarini, Y. C. Chow, L. Ciupik, P. Cogan, P. Colin, W. Cui, R. Dickherber, C. Duke, S. J. Fegan, J. P. Finley, G. Finnegan, P. Fortin, L. Fortson, A. Furniss, N. Galante, D. Gall, K. Gibbs, G. H. Gillanders, S. Godambe, J. Grube, R. Guenette, G. Gyuk, D. Hanna, J. Holder, D. Horan, C. M. Hui, T. B. Humensky, A. Imran, P. Kaaret, N. Karlsson, M. Kertzman, D. Kieda, J. Kildea, A. Konopelko, H. Krawczynski, F. Krenrich, M. J. Lang, S. Lebohec, G. Maier, S. McArthur, A. McCann, M. McCutcheon, J. Millis, P. Moriarty, R. Mukherjee, T. Nagai, R. A. Ong, A. N. Otte, D. Pandel, J. S. Perkins, F. Pizlo, M. Pohl, J. Quinn, K. Ragan, L. C. Reyes, P. T. Reynolds, E. Roache, H. J. Rose, M. Schroedter, G. H. Sembroski, A. W. Smith, D. Steele, S. P. Swordy, M. Theiling, S. Thibadeau, A. Varlotta, V. V. Vassiliev, S. Vincent, R. G. Wagner, S. P. Wakely, J. E. Ward, T. C. Weekes, A. Weinstein, T. Weisgarber, D. A. Williams, S. Wissel, M. Wood, and B. Zitzer. A connection between star formation activity and cosmic rays in the starburst galaxy M82. *Nature*, 462:770–772, December 2009.
- H. J. Voelk. The correlation between radio and far-infrared emission for disk galaxies - A calorimeter theory. *A&A*, 218:67–70, July 1989.
- M. S. Westmoquette, L. J. Smith, and J. S. Gallagher, III. Spatially resolved optical integral field unit spectroscopy of the inner superwind of NGC 253. *MNRAS*, 414:3719–3739, July 2011.

- P. K. G. Williams and G. C. Bower. Evaluating the Calorimeter Model with Broadband, Continuous Spectra of Starburst Galaxies Observed with the Allen Telescope Array. *ApJ*, 710:1462–1479, February 2010.
- A. S. Wilson and J. S. Ulvestad. Radio structures of Seyfert galaxies. IV - Jets in NGC 1068 and NGC 4151. *ApJ*, 263:576–594, December 1982.
- T. M. Yoast-Hull, J. S. Gallagher, III, E. G. Zweibel, and J. E. Everett. Active Galactic Nuclei, Neutrinos, and Interacting Cosmic Rays in NGC 253 and NGC 1068. *ApJ*, 780:137, January 2014.
- Tova M. Yoast-Hull, John E. Everett, III J. S. Gallagher, and Ellen G. Zweibel. Winds, clumps, and interacting cosmic rays in m82. *The Astrophysical Journal*, 768(1):53, 2013.
- M. S. Yun, N. A. Reddy, and J. J. Condon. Radio Properties of Infrared-selected Galaxies in the IRAS 2 Jy Sample. *ApJ*, 554:803–822, June 2001.